

N 64 28834
(ACCESSION NUMBER)

46
1 (PAGES)

1 (THRU)

MA5P CR 58614
(NASA CR OR TMX OR AD NUMBER)

0 (CODE)

O 3 (CATEGORY)

OTS PRICE

XEROX

\$

46024

MICROFILM

\$

WT 20-565

CONICAL AFTERBODY EFFECT ON THE
REARWARD STATIC STABILITY OF A
BLUNT-NOSED ENTRY VEHICLE AT
MACH 4.54

Edward Nierengarten
James Nichols

Robert E. Covey
Robert E. Covey, Chief
Aerodynamic Facilities Section

JET PROPULSION LABORATORY
CALIFORNIA INSTITUTE OF TECHNOLOGY
PASADENA, CALIFORNIA

February 13, 1964

Copyright © 1964
Jet Propulsion Laboratory
California Institute of Technology

Prepared Under Contract No. NAS 7-100
National Aeronautics & Space Administration

CONTENTS

I.	Introduction	1
II.	Model Description	1
III.	Wind Tunnel and Instrumentation	2
IV.	Test Procedure	3
V.	Data Reduction	3
VI.	Results	4
	Nomenclature	5
	References	6
	Table 1. Average aerodynamic parameters	7
	Figures	
	Plots	

FIGURES

1. Description of the seven complete configurations tested in a rearward-entry attitude
2. Model geometric parameters and direction of positive forces
3. Schlieren photographs of various models throughout the angle-of-attack range
4. Variation of C_{m_a} with cone-angle and cone-length ratio

PLOTS

Plot No.	Mach No.	P_T (cm Hg)	σ (deg)	$\ell - \ell'$ (in.)	ℓ' (in.)	ℓ (in.)	Fixed Model Characteristics	Run No.
1	4.54	328.0	35	variable	variable	≈ 2.86	common angle and vertex position	4,6,8
2			25	variable	≈ 2.3	variable	common angle, after-body length	10,12,14
3				variable	≈ 1.87	variable	common base position	2,12
4				variable	variable	≈ 2.86	common vertex position	2,4,6,8,14

I. INTRODUCTION

Wind-tunnel Test 20-565 was a test of a typical entry vehicle with a conical body mounted upstream from the base of the vehicle by means of a cylindrical element. The purpose of the test was to investigate the effects on static stability of interference at a high supersonic velocity when a conical body is mounted upstream from the base of an entry vehicle. All configurations were tested in the JPL 20-in. supersonic wind tunnel at an angle-of-attack range from 0 to 29 deg. The approximate aerodynamic parameters for the test were Mach No. 4.54, total pressure 328.0 cm Hg, and a corresponding Reynolds No./in. of 0.34×10^6 . 28634

The model configuration comprised a conical afterbody, attached to a spherical-segment forebody by means of a cylindrical element, which has a diameter one-fourth the diameter of the forebody. It should be noted that the terms, afterbody and forebody, as used in this Report denote respective locations considering the spherical segment upstream of the conical body. For this test, however, the model attitude was reversed 180 deg, so that the denoted forebody and afterbody are acting as the afterbody and forebody, respectively.

Forces and moments, measured by means of a strain-gage balance, were obtained for the complete configuration which was tested in a rearward-entry attitude.

The test* was conducted at the Jet Propulsion Laboratory (JPL) for Section 373 of JPL on July 29, 1963. Author

II. MODEL DESCRIPTION

The models are shown in Fig. 1. Three types of conical afterbodies were tested in combination with the spherical-segment forebody. The afterbodies, classified according to cone angle, were 25, 35, and 45 deg.

The vertex position for most of the complete models was that determined by the vertex position of a full 35-deg conical afterbody; this is referred to as the common vertex position.

* Symbols used in this Report are defined in the Nomenclature.

The 25-deg conical afterbody had one length and three distinct vertex positions. The length was fixed as that length which was 80% of the distance from the common vertex to the base of the forebody. One position of the 25-deg conical afterbody was that of the common vertex position (Fig. 1a). The second vertex position was such that the base of the 25-deg afterbody was in the same location as the base of the 45-deg afterbody at the common vertex position. With this arrangement, while the afterbody length remained the same, the distance from the new vertex position to the base of the forebody changed, so that the afterbody length was now only 55.2% of this distance (Fig. 1b). The third vertex position was that which allowed the 25-deg conical envelope to enclose the forebody. At this position, the afterbody length was 53.4% of the distance from the vertex to the forebody base (Fig. 1c).

The 35-deg conical afterbody had 3 distinct lengths and one common vertex position. The three lengths were 100%, 66.6%, and 41.5% of the distance from the common vertex to the forebody base (Fig. 1d, 1e, 1f).

The 45-deg conical afterbody was located at the common vertex position having a length equal to 35% of the distance from the common vertex to the forebody base (Fig. 1g).

The complete model configuration was designated by the cone angle of the afterbody (σ) and the ratio of the afterbody length (ℓ') to the distance from the forebody base to the particular vertex position (ℓ), ℓ'/ℓ ; i. e.: $\sigma-\ell'/\ell$ (Fig. 2).

III. WIND TUNNEL AND INSTRUMENTATION

Reference 1 describes the construction and operating conditions of the 20-in. supersonic wind tunnel. The wind tunnel has a nominal test-section size of 20 in. square, a Mach range from 1.3 to 5.0, a flexible-plate nozzle, and operates with continuous flow. Table 1 presents representative values of the test-section flow parameters for the Mach number at which this test was conducted.

A six-component, internal, strain-gage balance was used to measure force-and-moment data.

IV. TEST PROCEDURE

Prior to actual test operations, measurements were made to determine the position of the model, the deflection constants, and balance tares. During the test, data points were obtained at successive values of angle of attack. These data points were plotted vs angle of attack and any data which appeared questionable were checked before the conclusion of the run. At least one data point was checked even if all data appeared correct.

Schlieren photographs (Fig. 3a through g) were made of each model for Mach No. 4.54 at 4, 8, 12, 18, 22, 26, and 29 deg angle of attack, respectively. Two Schlieren photographs were taken of model 25-534 at $\alpha = 18$ deg to show the change in shock pattern on the model at 18 deg when this angle was approached from 0 deg and 29 deg angle of attack (Fig. 3f).

V. DATA REDUCTION

The force-and-moment data were reduced to dimensionless coefficients in the pitch-axis and wind-axis systems. The coefficients were obtained as follows:

$$\text{force coefficient} = \frac{\text{force}}{qA}$$

$$\text{moment coefficient} = \frac{\text{moment}}{qAD}$$

where

$$q = \text{free-stream dynamic pressure} = 3.00 \text{ (psia)}$$

$$A = \text{reference area} = 12.56 \text{ (in.}^2\text{)}$$

$$D = \text{reference length} = 4.0 \text{ (in.)}$$

and the point about which the moments were measured was the model base, on the model centerline. The axial-force coefficient was corrected to eliminate

the base-drag increment due to the differential between base pressure and free-stream static pressure.

The coefficients were obtained on a digital computer by a standardized series of formulae as indicated in Ref. 2 and 3.

The coefficients are defined in the Nomenclature, and the coefficient sign conventions are shown in Fig. 2.

VI. RESULTS

The results of this test are shown in Plot Series 1a-g through 4a-g.* Tests with the 35-deg cone show that, with a given cone angle and vertex position, reducing the cone length by cutting off the base of the cone causes the vehicle to become more stable (Plot 1b). Decreasing the cone angle, while keeping the vertex position constant, tends to increase the stability (Plot 4b). With a given cone geometry, i. e., cone angle and cone length, decreasing the gap distance between the forebody base and the cone increases the stability (Plot 2b).

Newtonian theory predicts very well the static stability of the 35-deg full cone but is inadequate for the other configurations tested (Fig. 4).

*Also numbered from 1 through 28 in the lower left-hand corner of the ozalid plot pages of this Report.

NOMENCLATURE

A	reference area (12.56 in. ²)
A_b	area of base of model (12.56 in. ²)
CA	axial-force coefficient (axial force/qA -CPB)
CD	drag coefficient, $CA \cos \alpha + CN \sin \alpha$
CL	lift coefficient, $CN \cos \alpha - CA \sin \alpha$
CM	pitching-moment coefficient about reference C. G. at base of model, moment/qAD
CN	normal-force coefficient, normal force/qA
CPB	base-drag coefficient $\left[(P - P_b) A_b \right] / qA$
d	diameter of the circle inscribed on the vertical plane at the base position by extending the conical surface of the afterbody at each vertex position to the plane (in.)
D	reference length, diameter of base of model (4.0 in.)
ℓ	distance from model base to the vertex position (in.)
ℓ'	afterbody length (in.)
M	Mach No.
P	static pressure (psia)
P_b	base pressure (psia)
q	free-stream dynamic pressure (3.00 psia)
XCP/D	center-of-pressure location on longitudinal axis of body measured from base of model, positive toward vertex position (CM/CN)
α	angle of attack, alpha (deg)
σ	cone half-angle (deg)

REFERENCES

1. Jet Propulsion Laboratory, California Institute of Technology. Wind-Tunnel Facilities at the Jet Propulsion Laboratory, Wind-Tunnel Staff. Pasadena, California, JPL, April 18, 1961. (Technical Release No. 34-257) UNCLASSIFIED
2. Jet Propulsion Laboratory, California Institute of Technology. Standard Data-Reduction Procedures for Use in the JPL Wind Tunnels, Wind-Tunnel Staff. Pasadena, California, JPL, June 8, 1962. (Internal Memorandum JPL WT G-T14) UNCLASSIFIED
3. Jet Propulsion Laboratory, California Institute of Technology. Equations for Wind-Tunnel-Force Data Reduction, Wind-Tunnel Staff. Pasadena, California, JPL, April 19, 1957. (Internal Memorandum SWT G-T3) UNCLASSIFIED

Table 1. Average aerodynamic parameters

Parameter	Mach Number
	4.54
Static pressure (psia)	0.21
Stagnation pressure (psia)	63.17
Dynamic pressure (psia)	3.00
Reynolds number (per in. $\times 10^{-6}$)	0.34

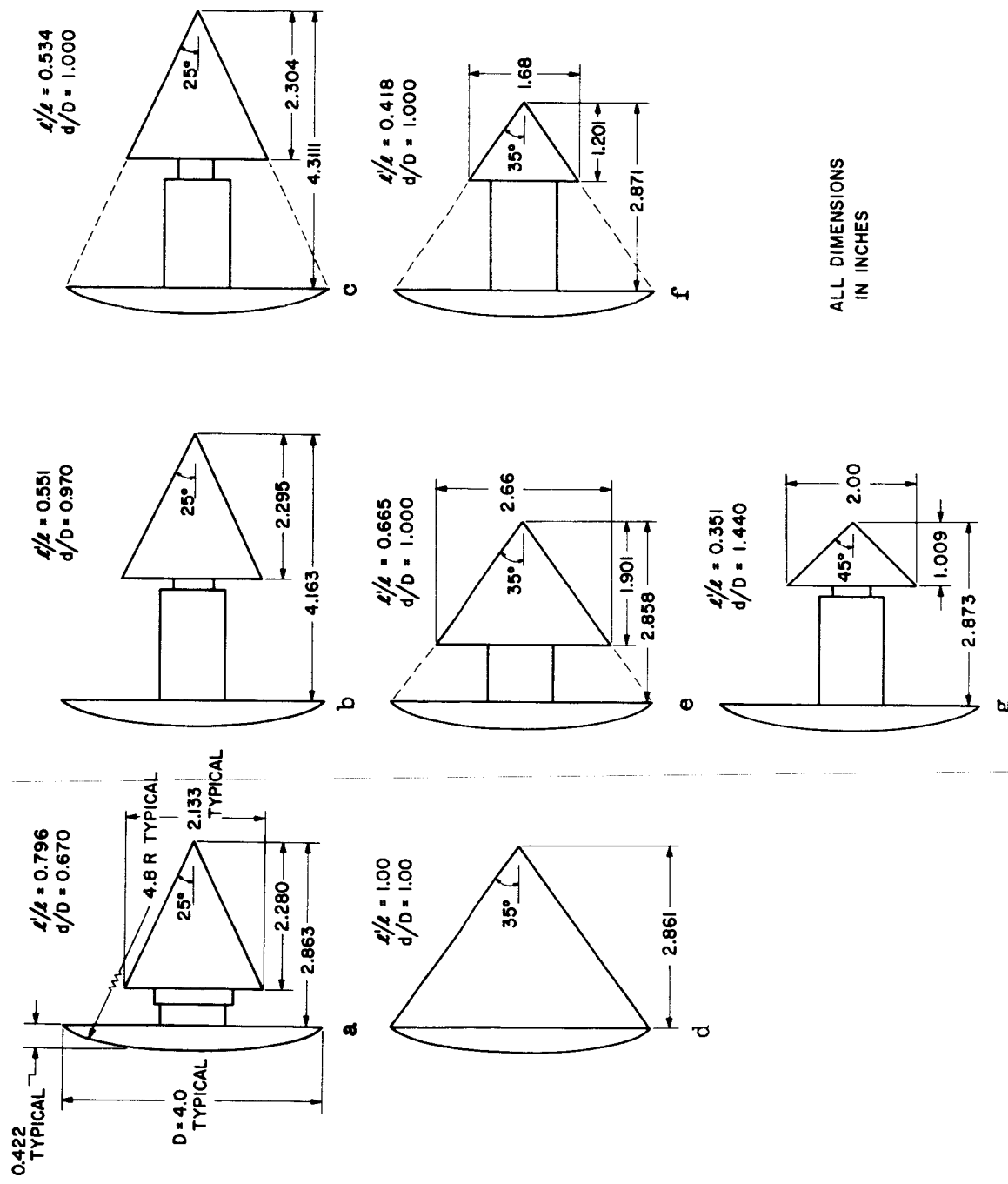
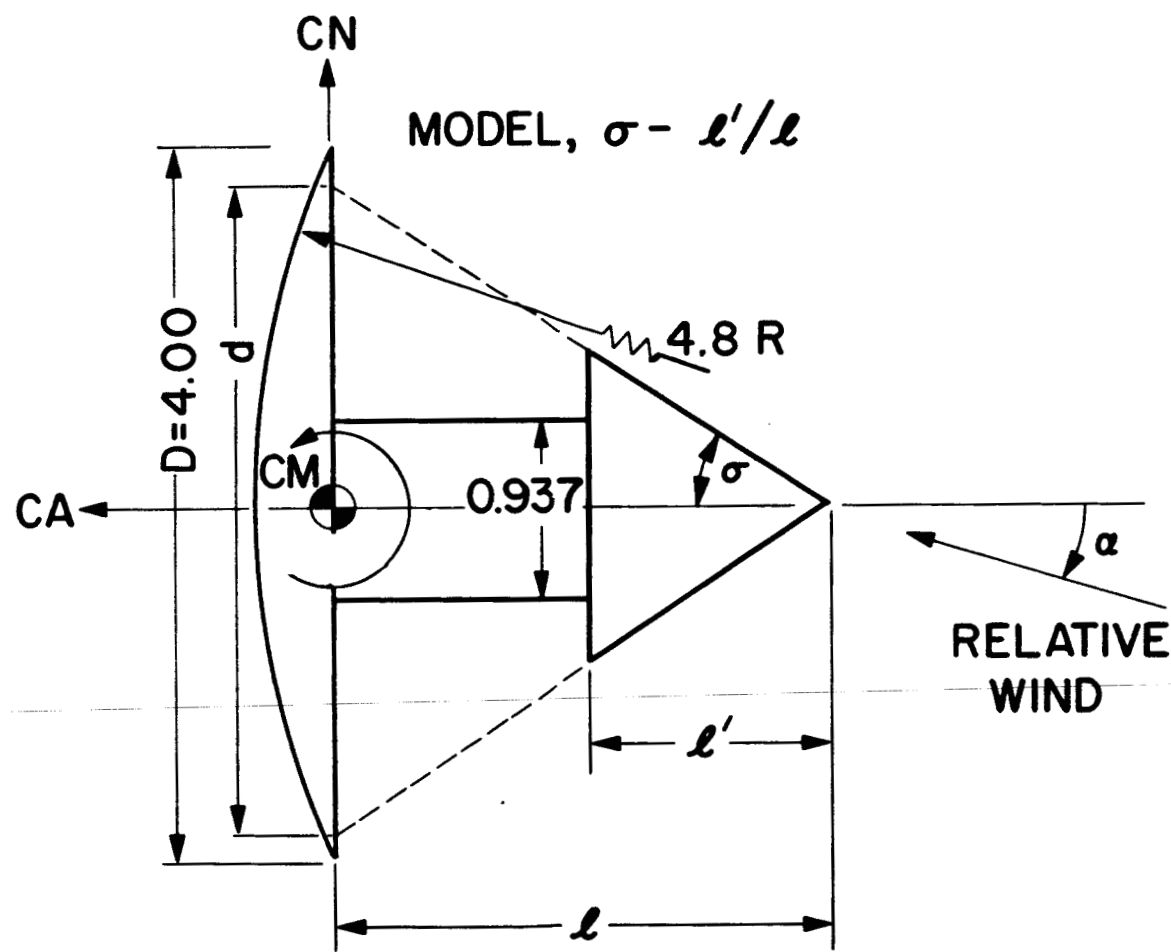


Fig. 1 Description of the Seven Complete Configurations Tested in a Rearward Entry Attitude.



(All Dimensions in Inches)

Fig. 2 Model Geometric Parameters and Direction of Positive Forces.

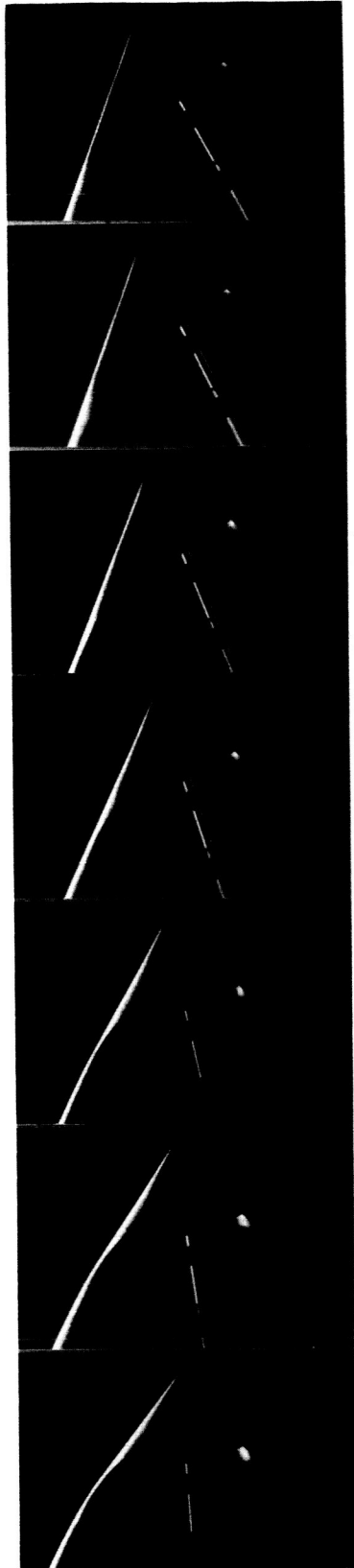


Fig. 3a Schlieren photos of model 35-100 throughout the angle of attack range.



Fig. 3b Schlieren photos of model 35-666 throughout the angle of attack range.

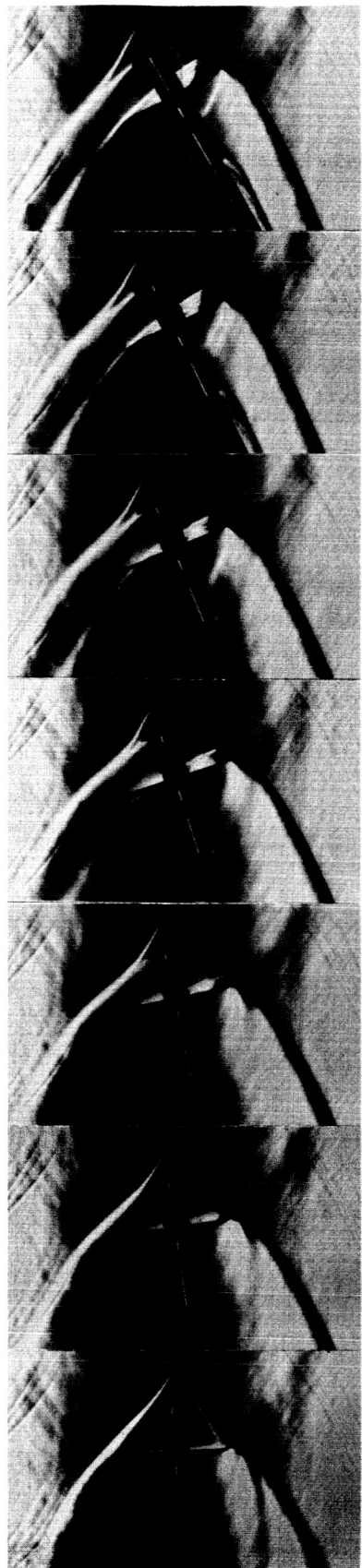
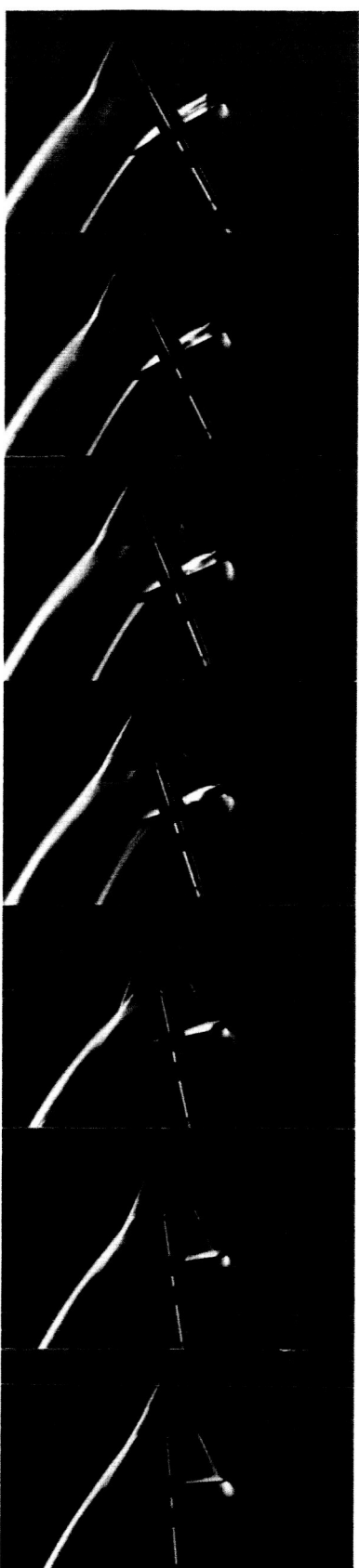


Fig. 3c Schlieren photos of model 35-415 throughout the angle of attack range.



Fig. 3d Schlieren photos of model 25-80 throughout the angle of attack range.



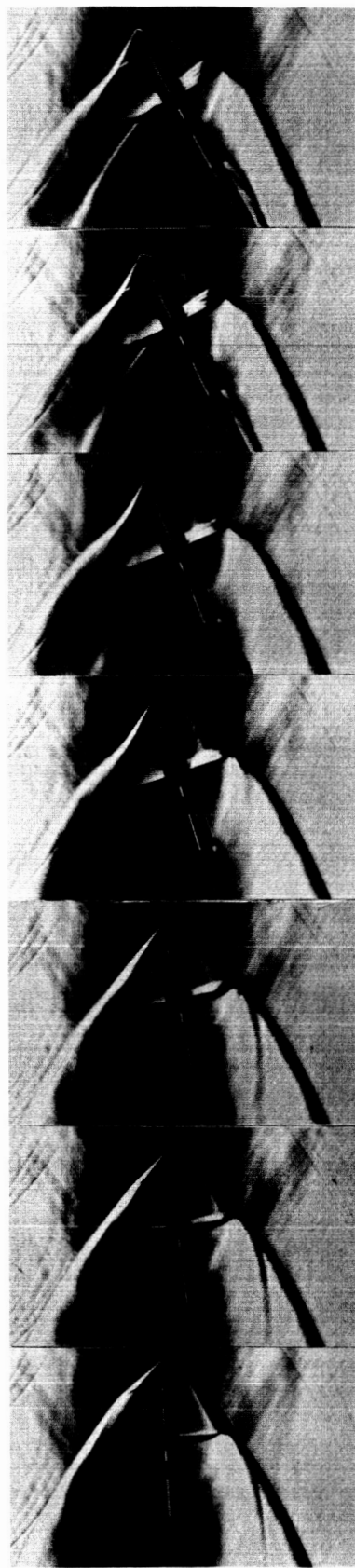
$\alpha = 4^\circ$ 8° 12° 18° 22° 26° 29°

Fig. 3e Schlieren photos of model 25-552 throughout the angle of attack range.



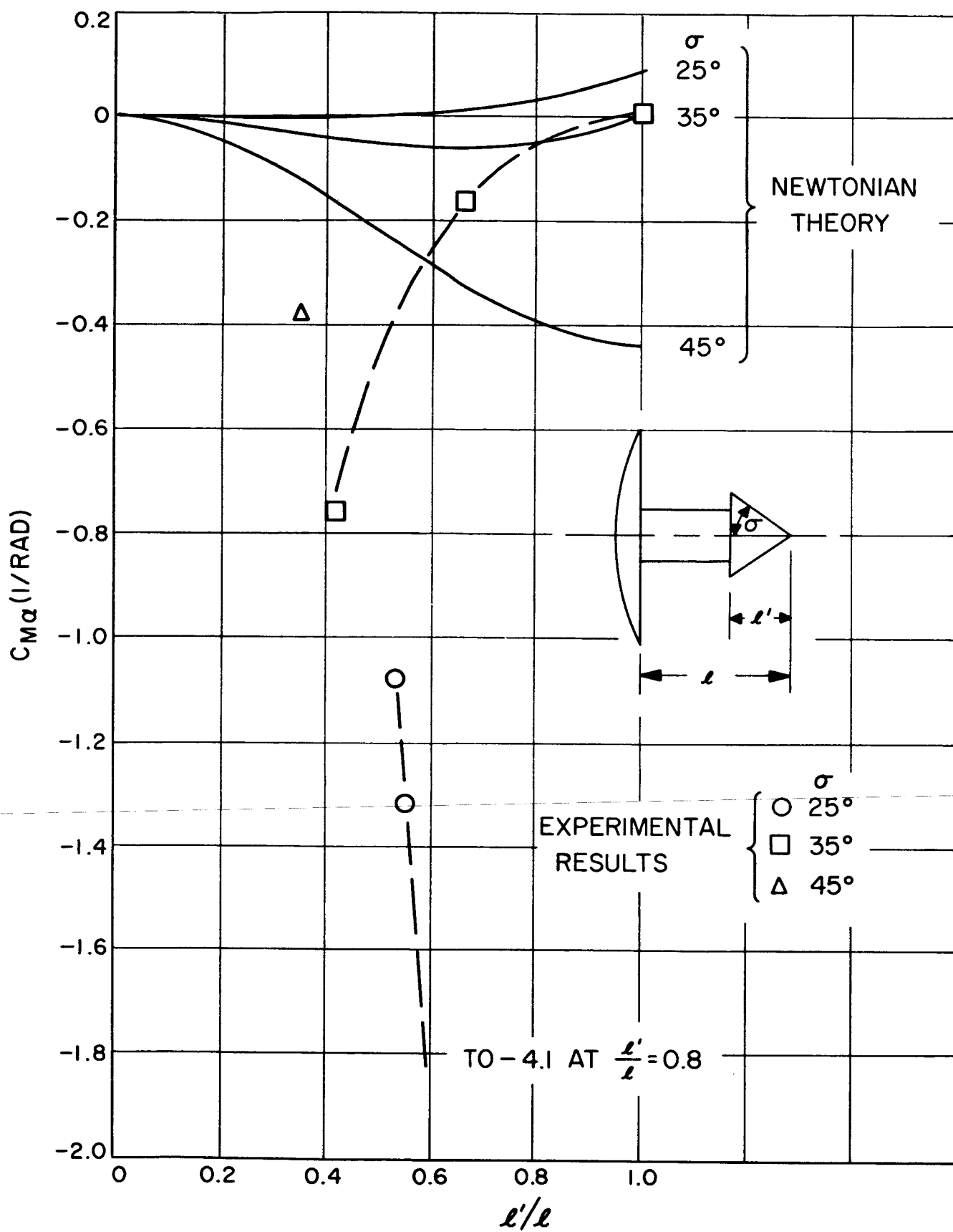
$\alpha = 4^\circ$ 8° 12° $+18^\circ$ approached from 0° 22° 26° 29° -18° approached from 29°

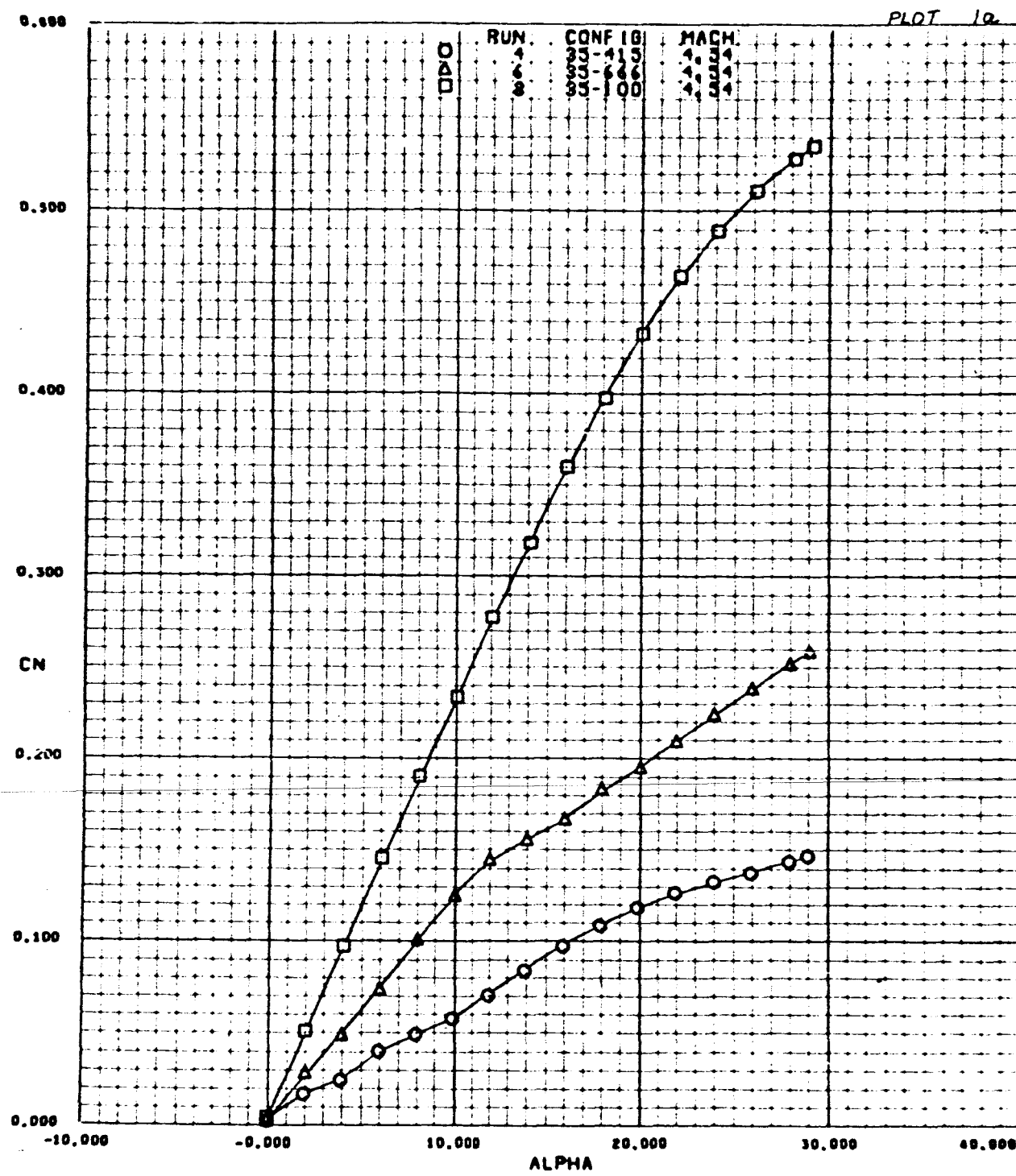
Fig. 3f Schlieren photos of model 25-534 throughout the angle of attack range.



$\alpha = 4^\circ$ 8° 12° 18° 22° 26° 29°

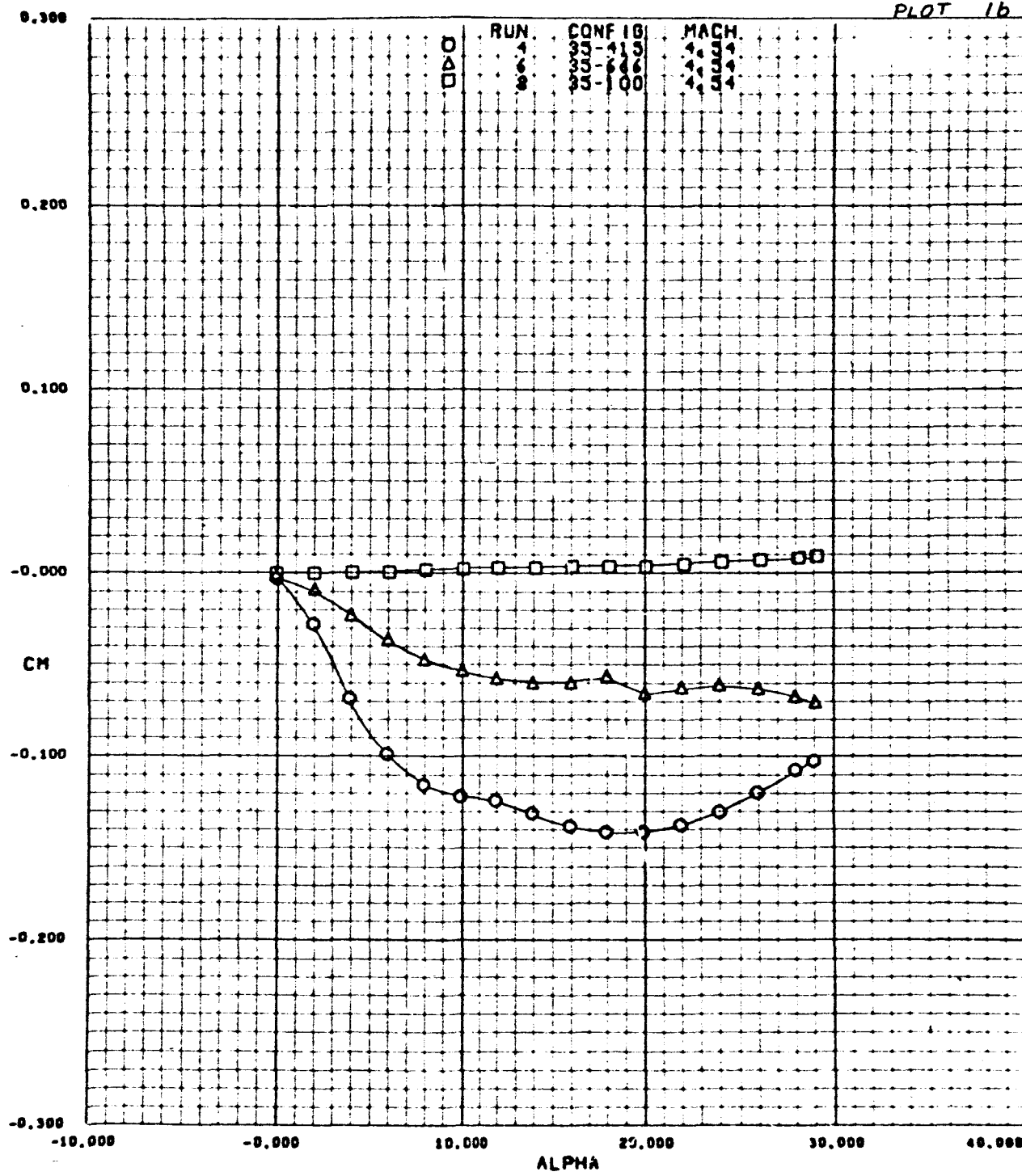
Fig. 3g Schlieren photos of model 45-35 throughout the angle of attack range.

Fig. 4 Variation of $C_{m\alpha}$ with Cone-Angle and Cone-Length Ratio.

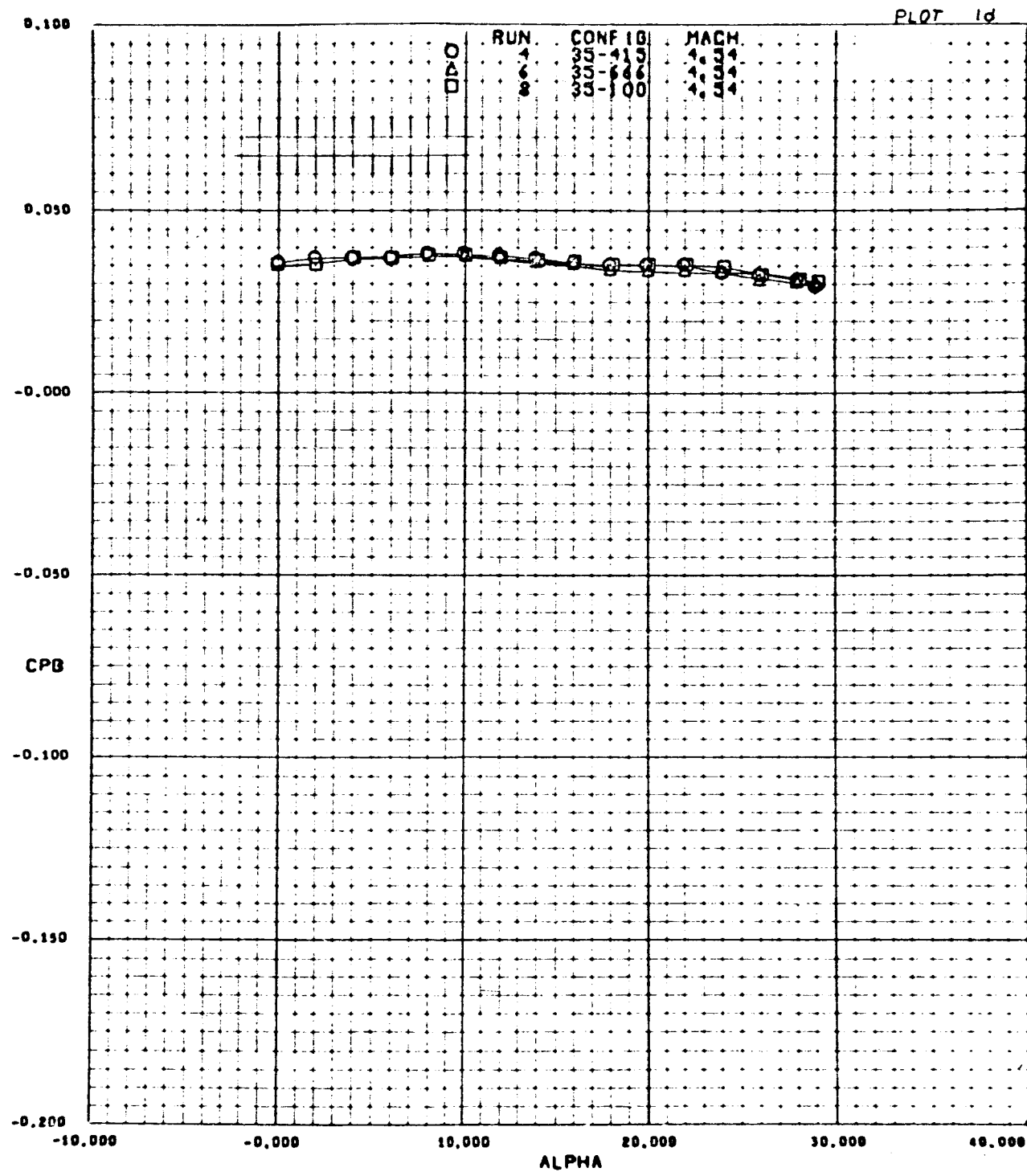


JPL WT 20-565

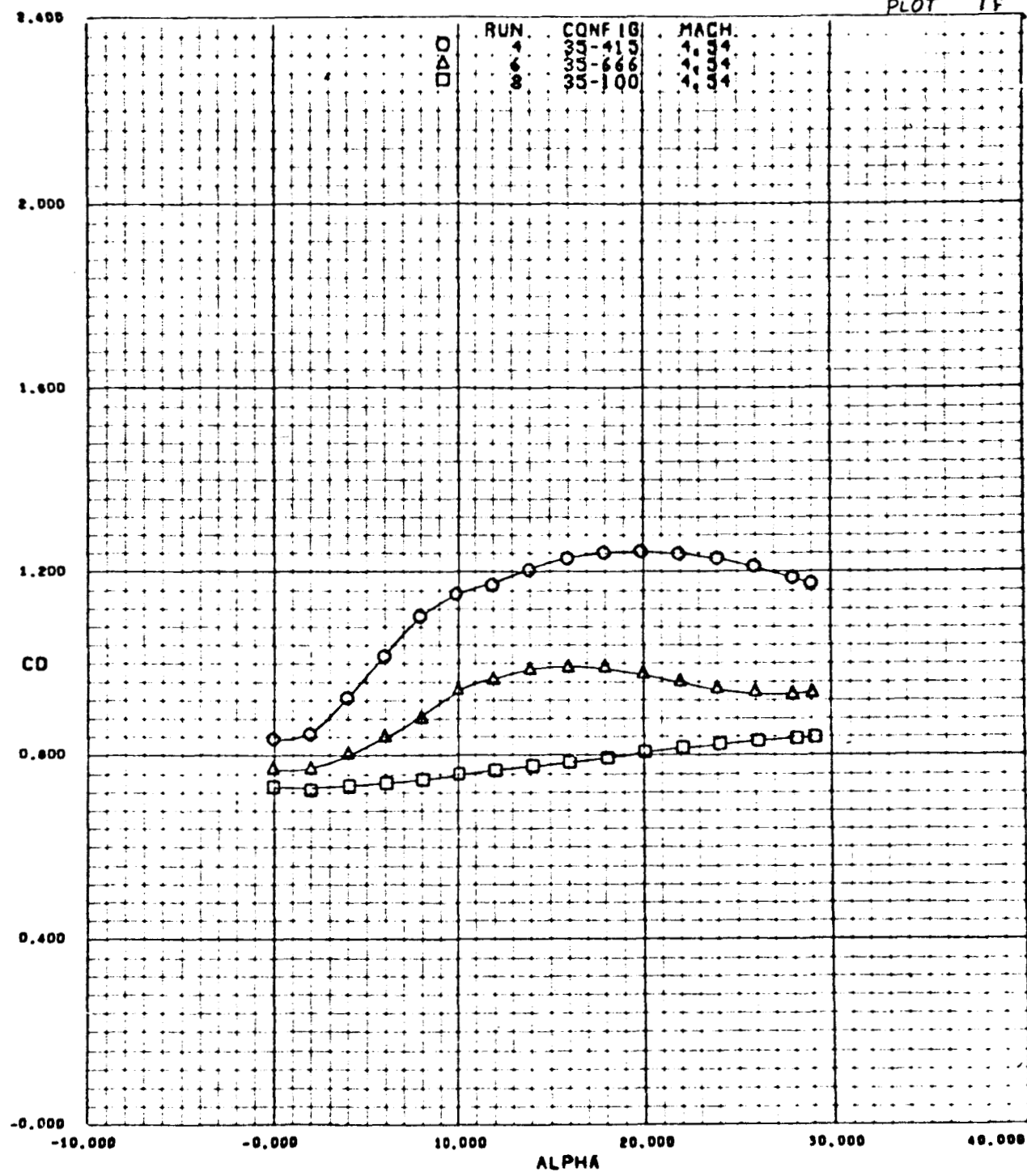
PLOT 1b



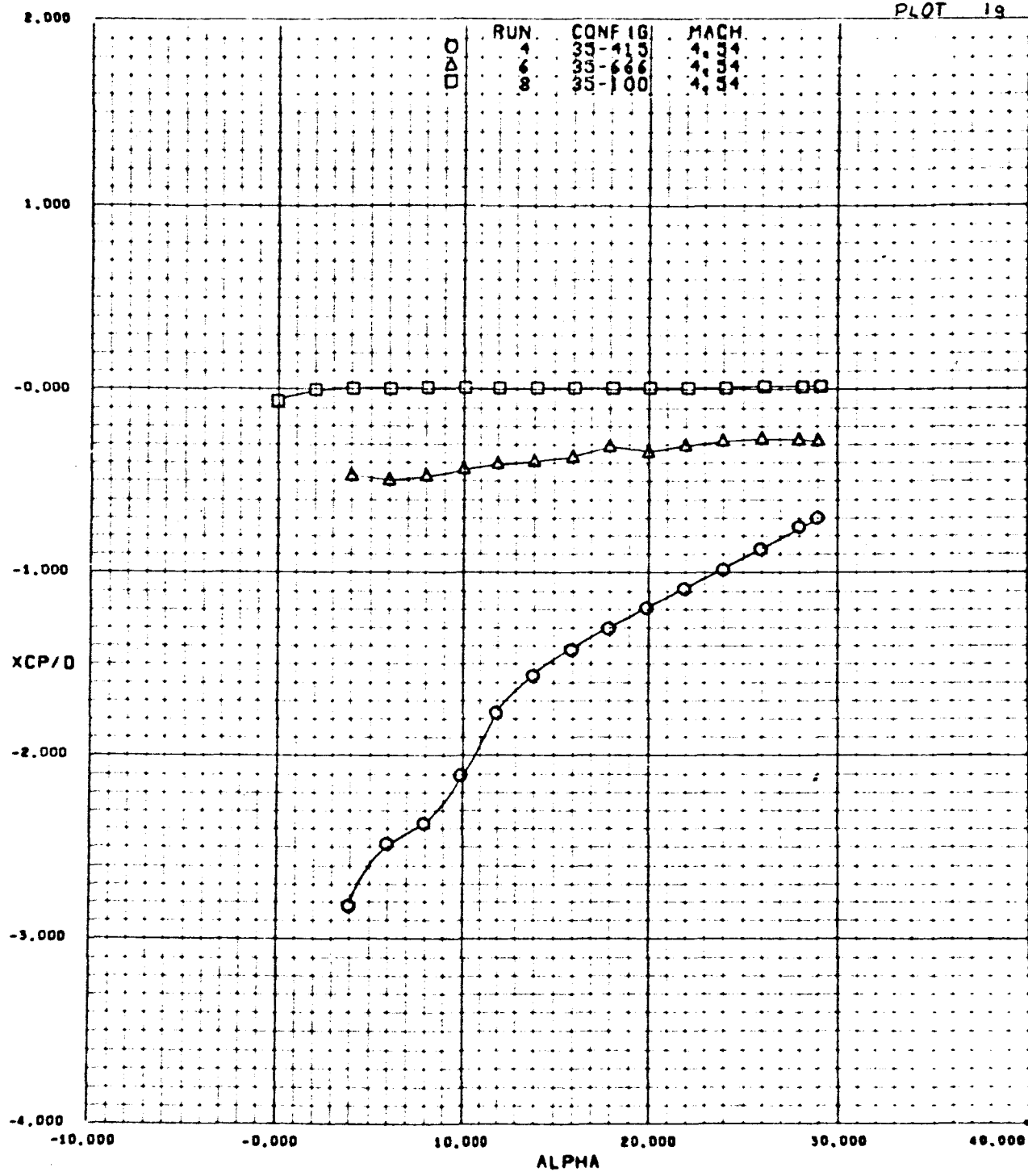
JPL WT 20-565



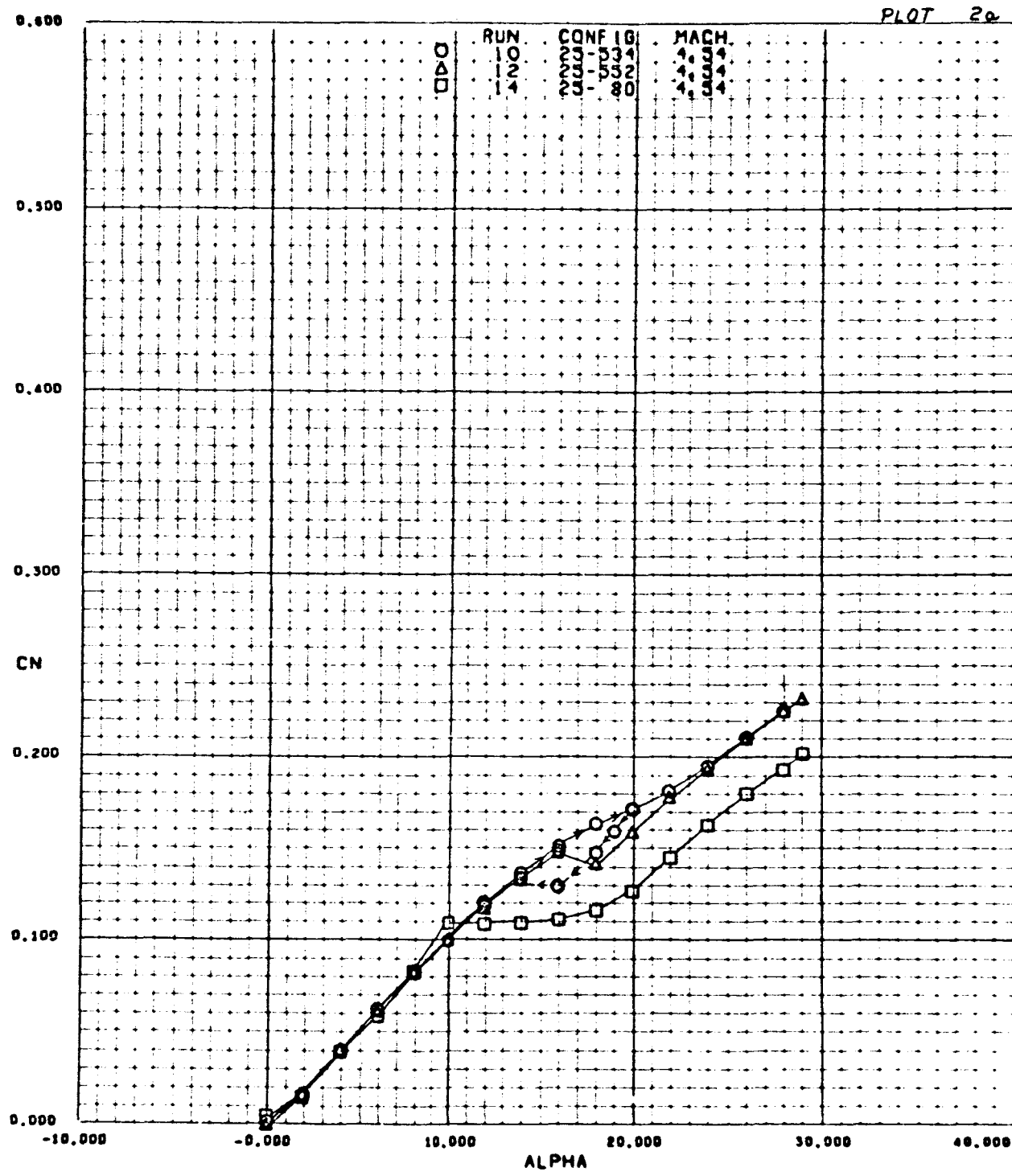
PLOT 1 F



PLOT 19

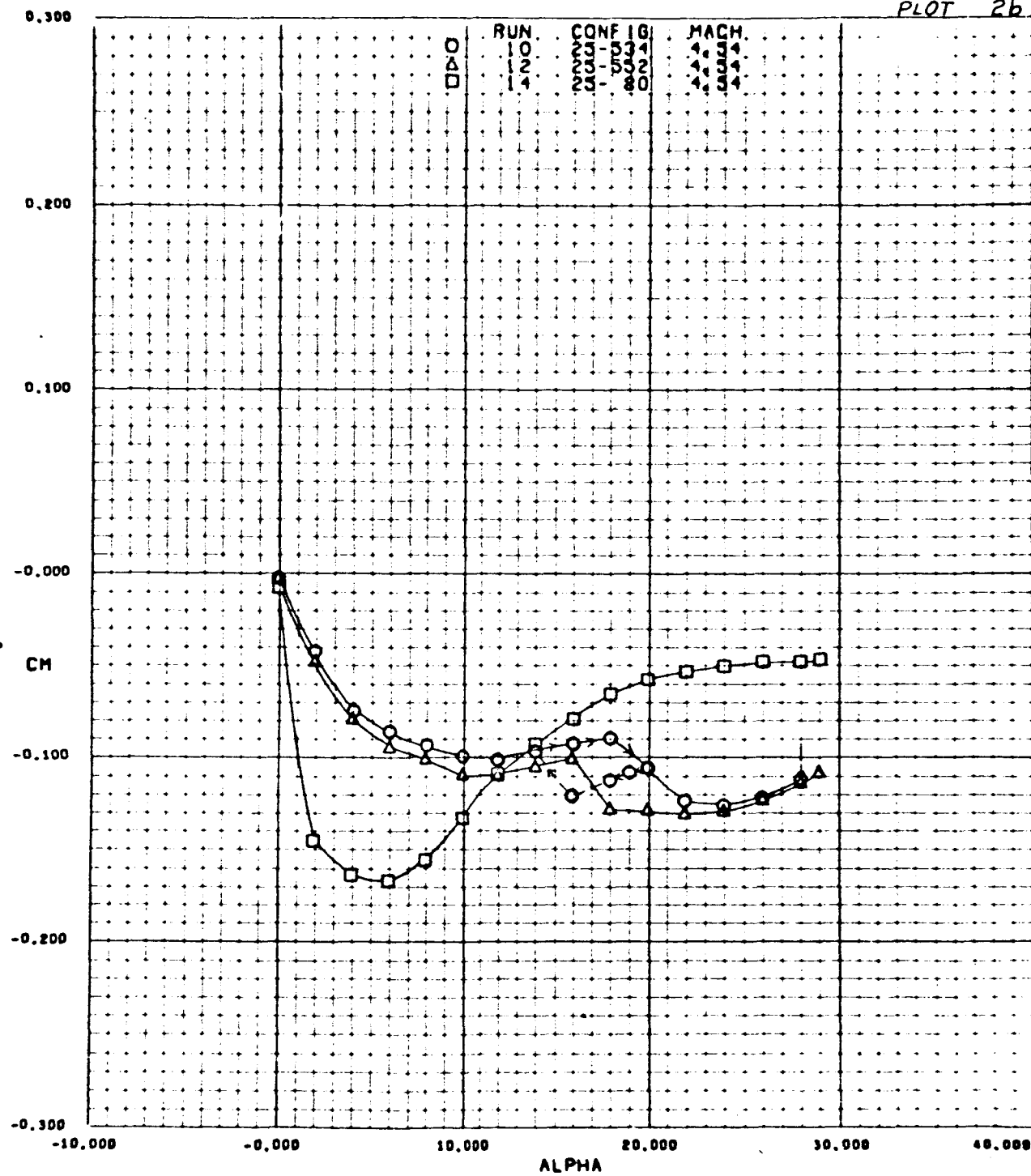


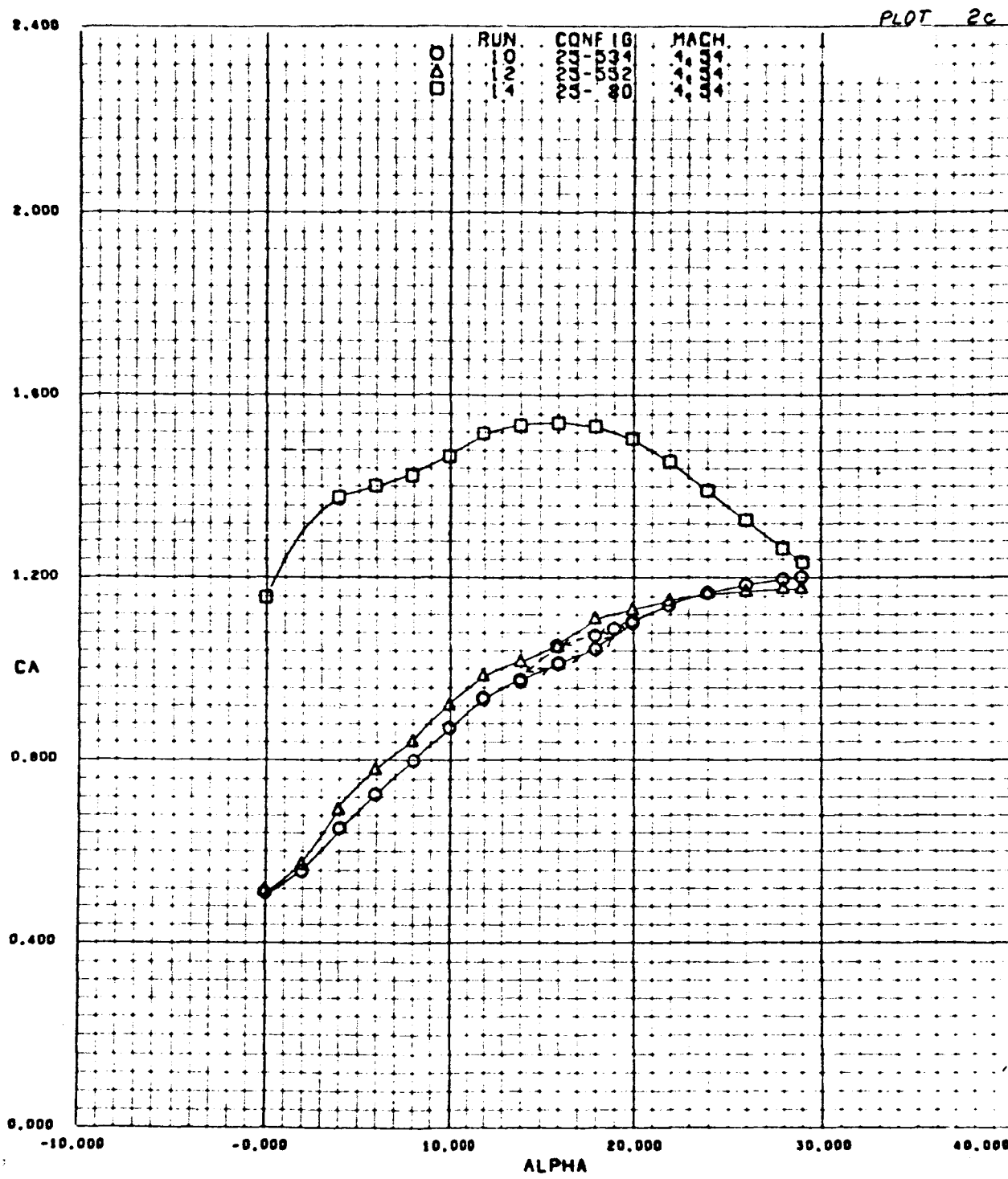
JPL WT 20-565



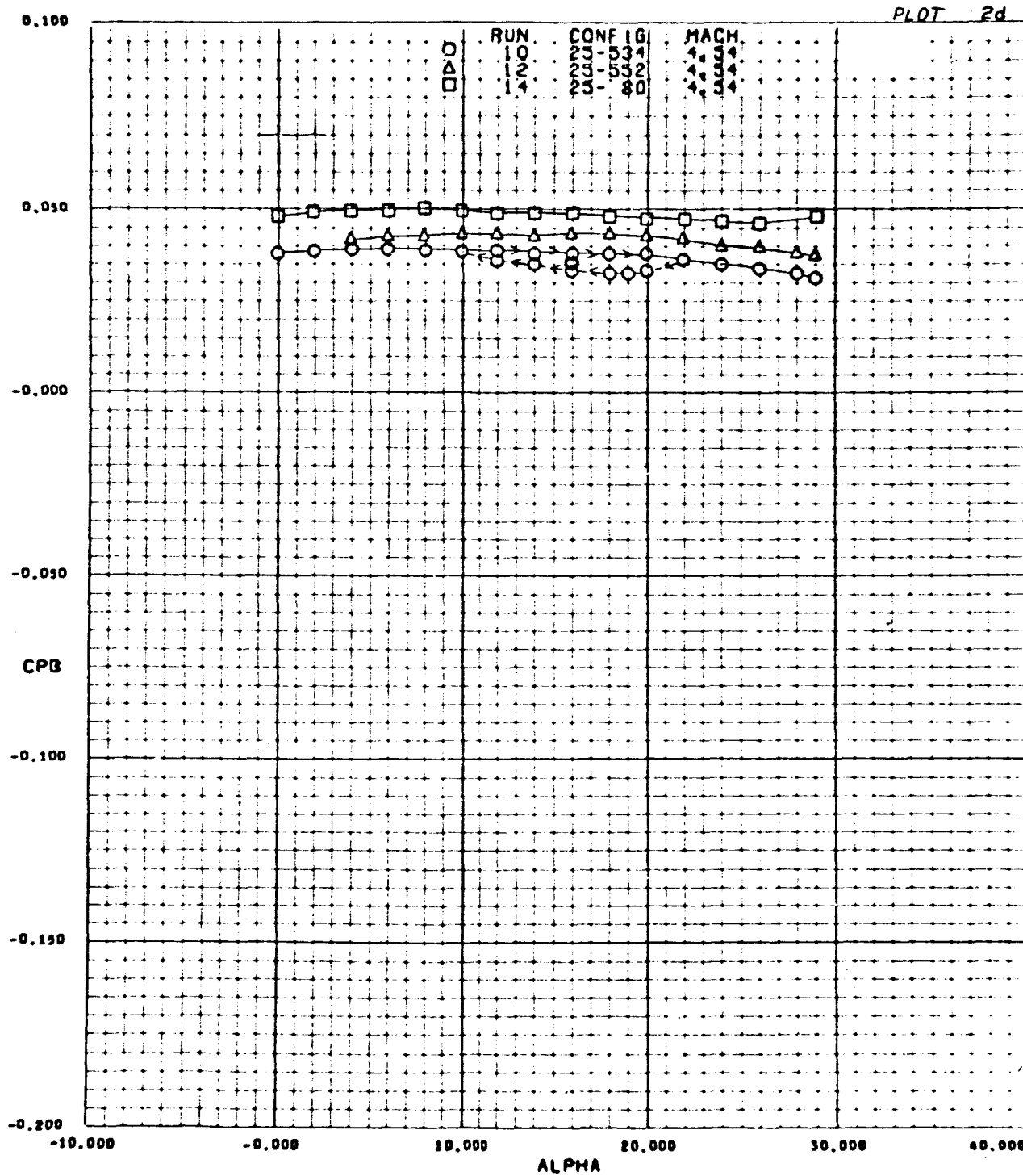
JPL WT 20-565

PLOT 2b

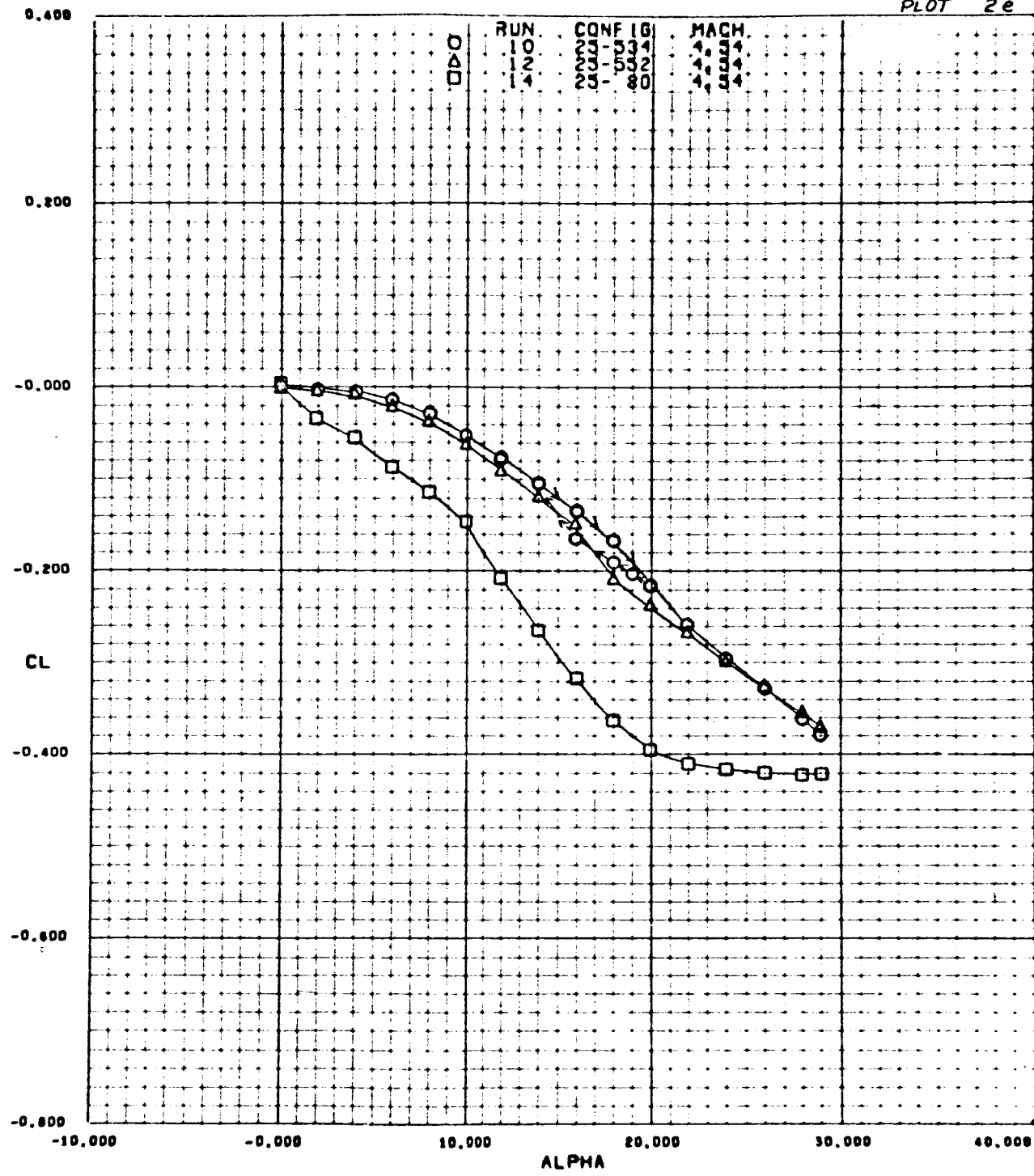




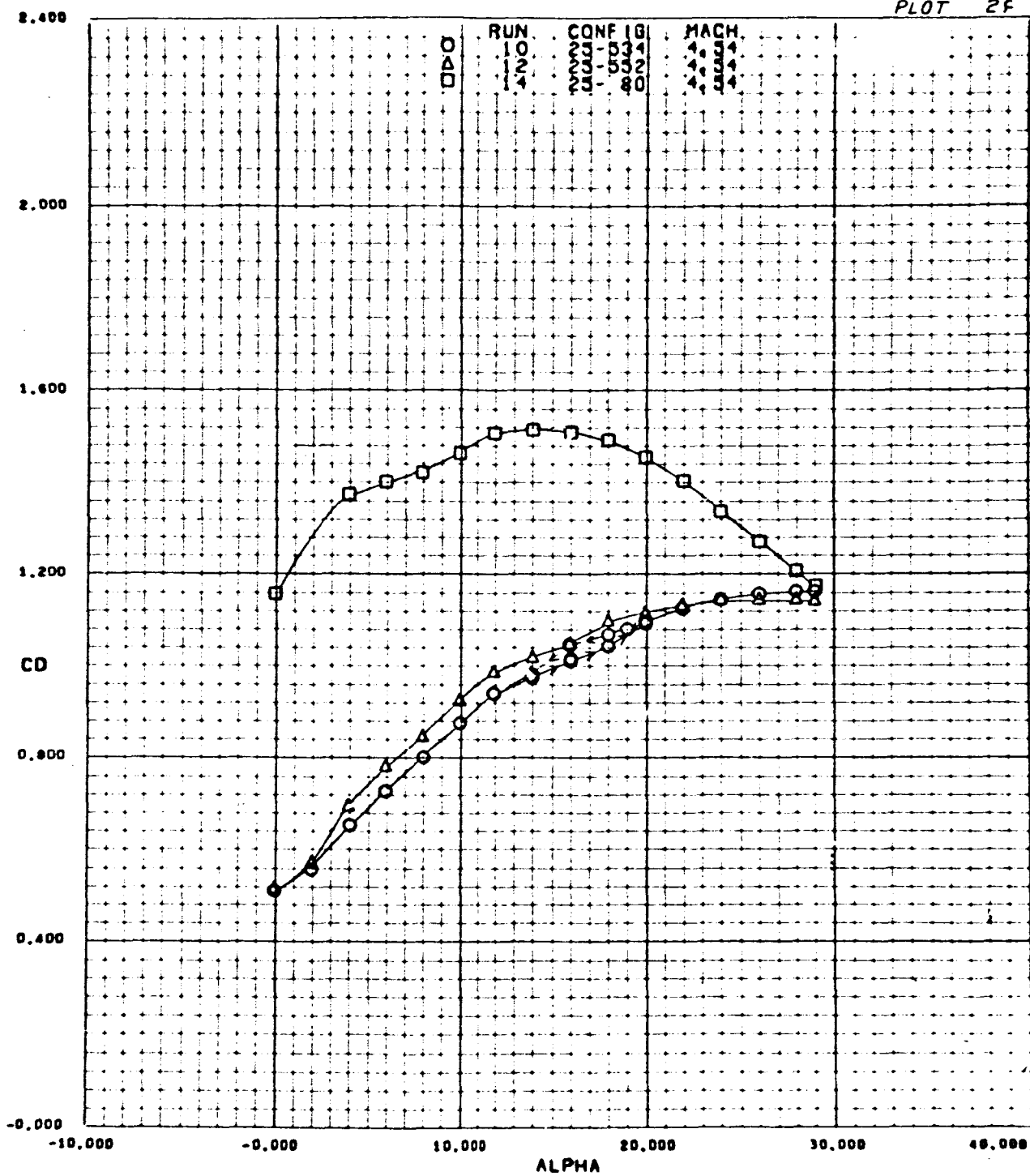
JPL WT 20-565



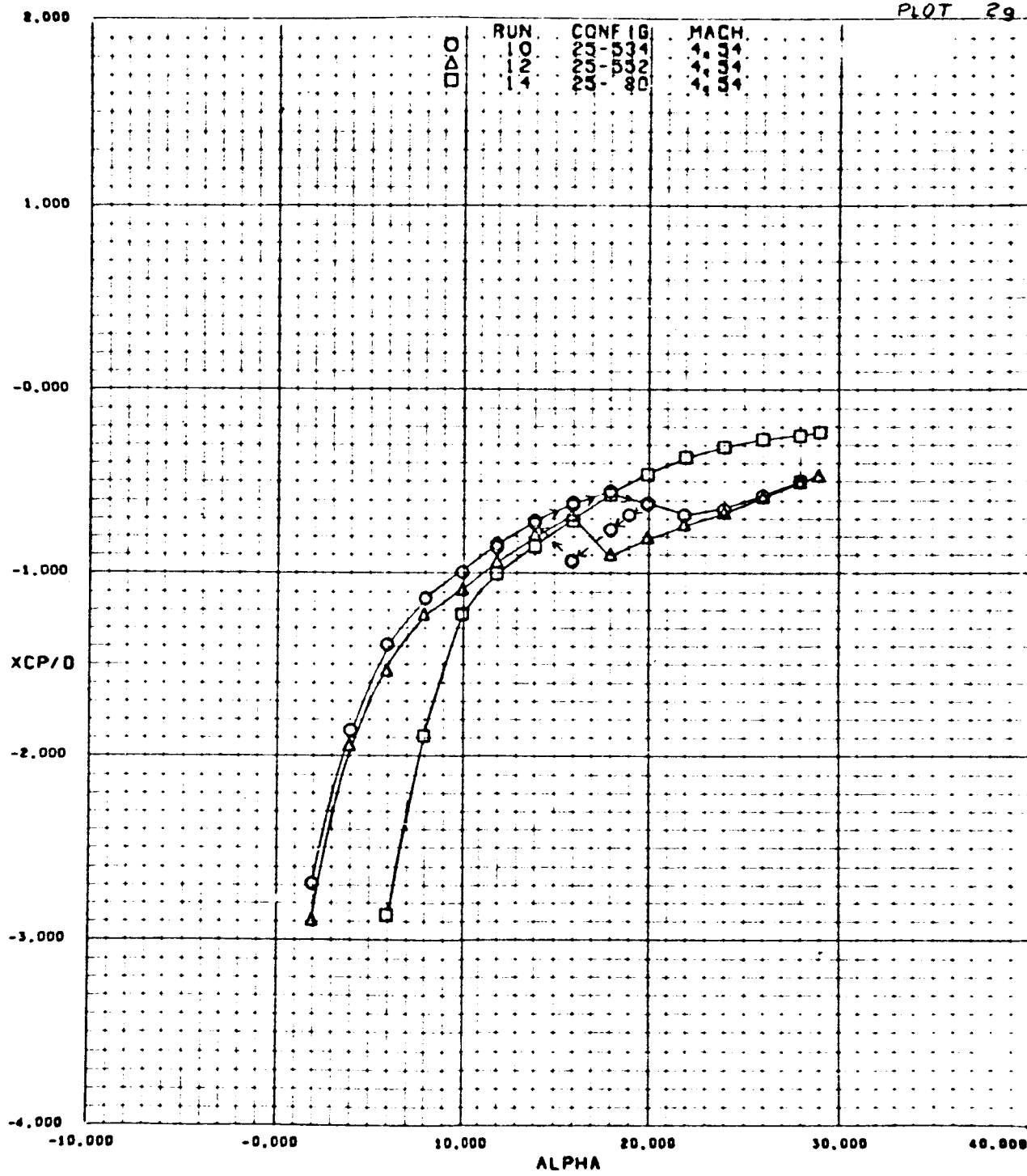
PLOT 2e

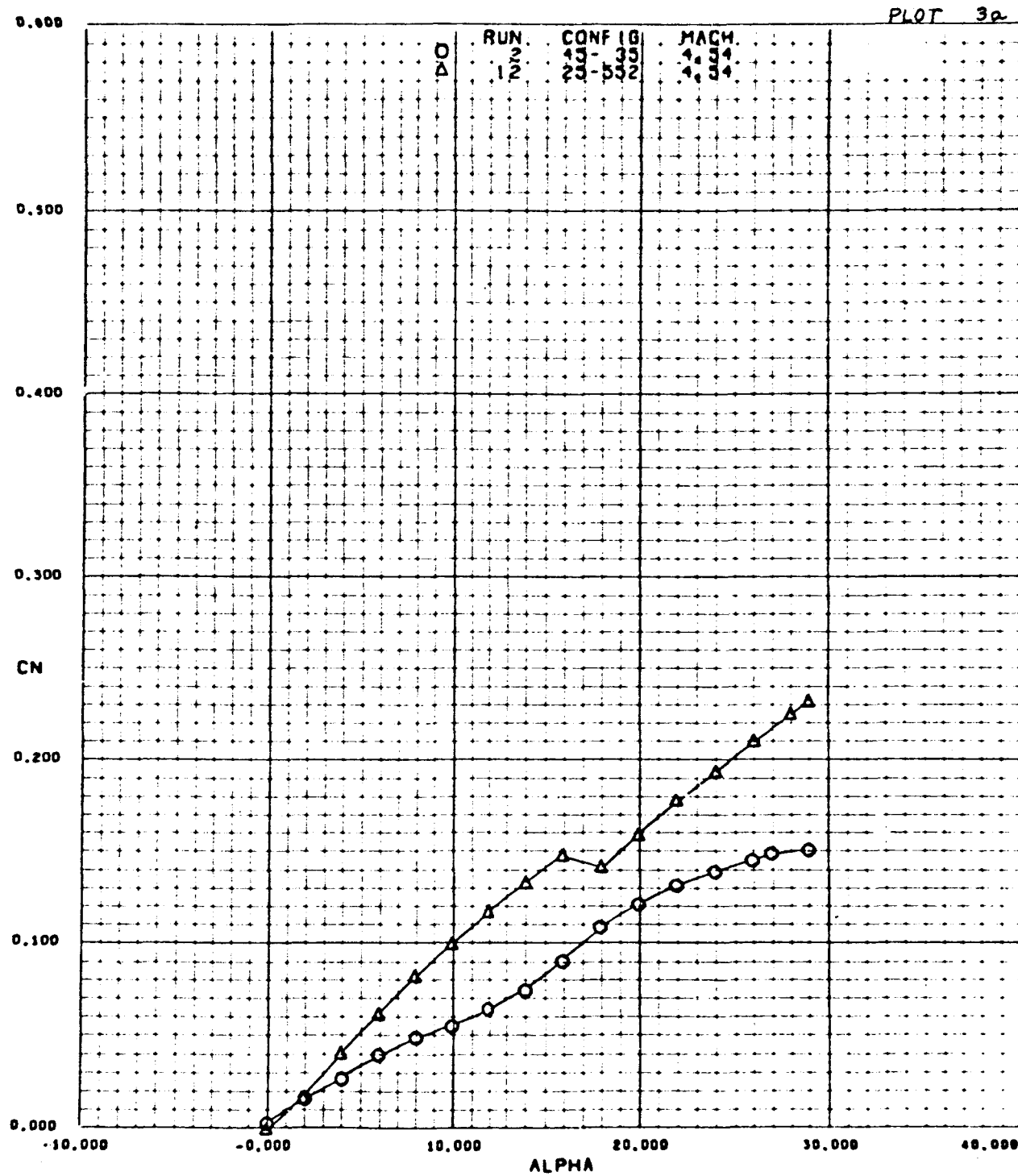


PLOT 2F

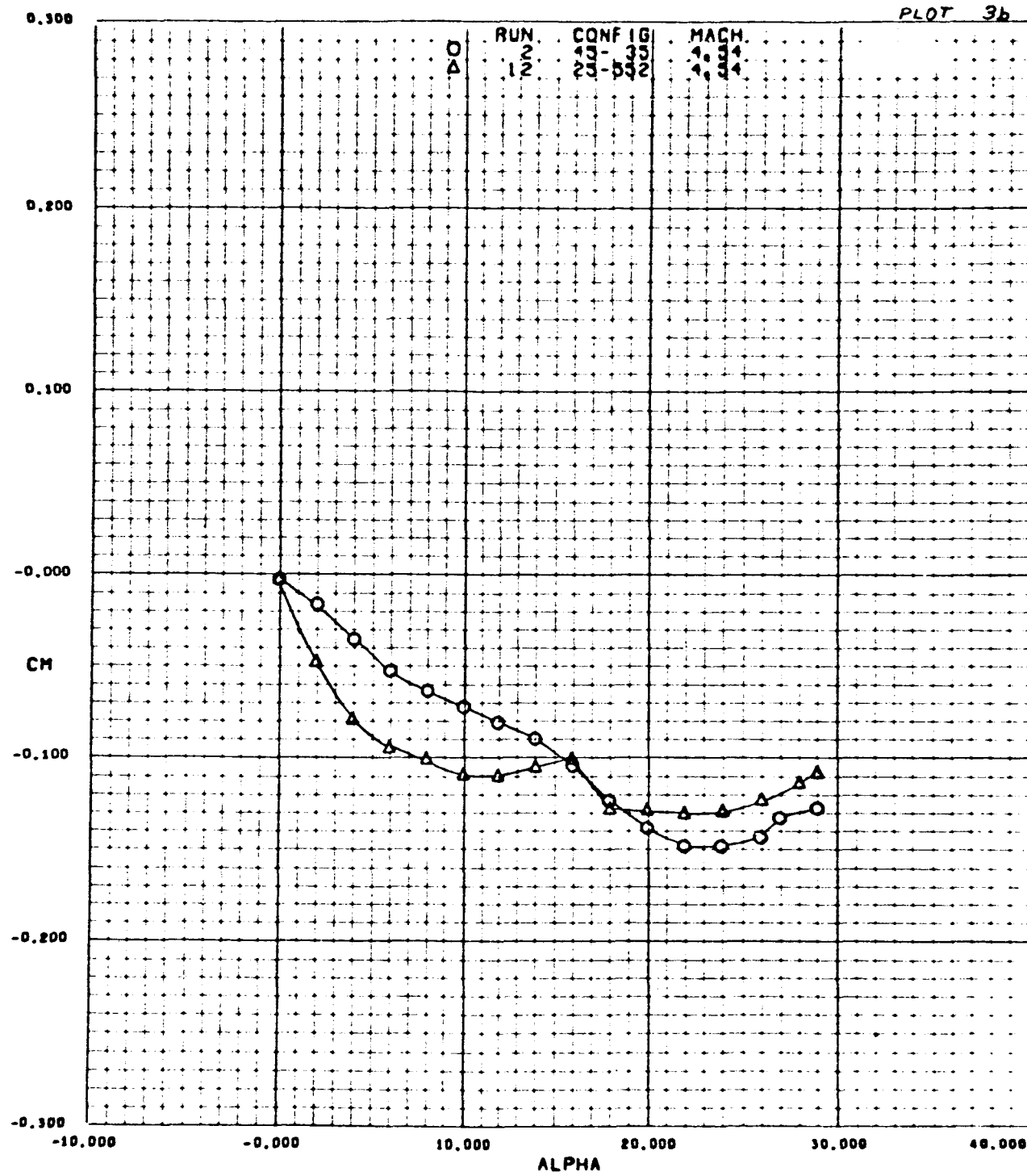


PLOT 29

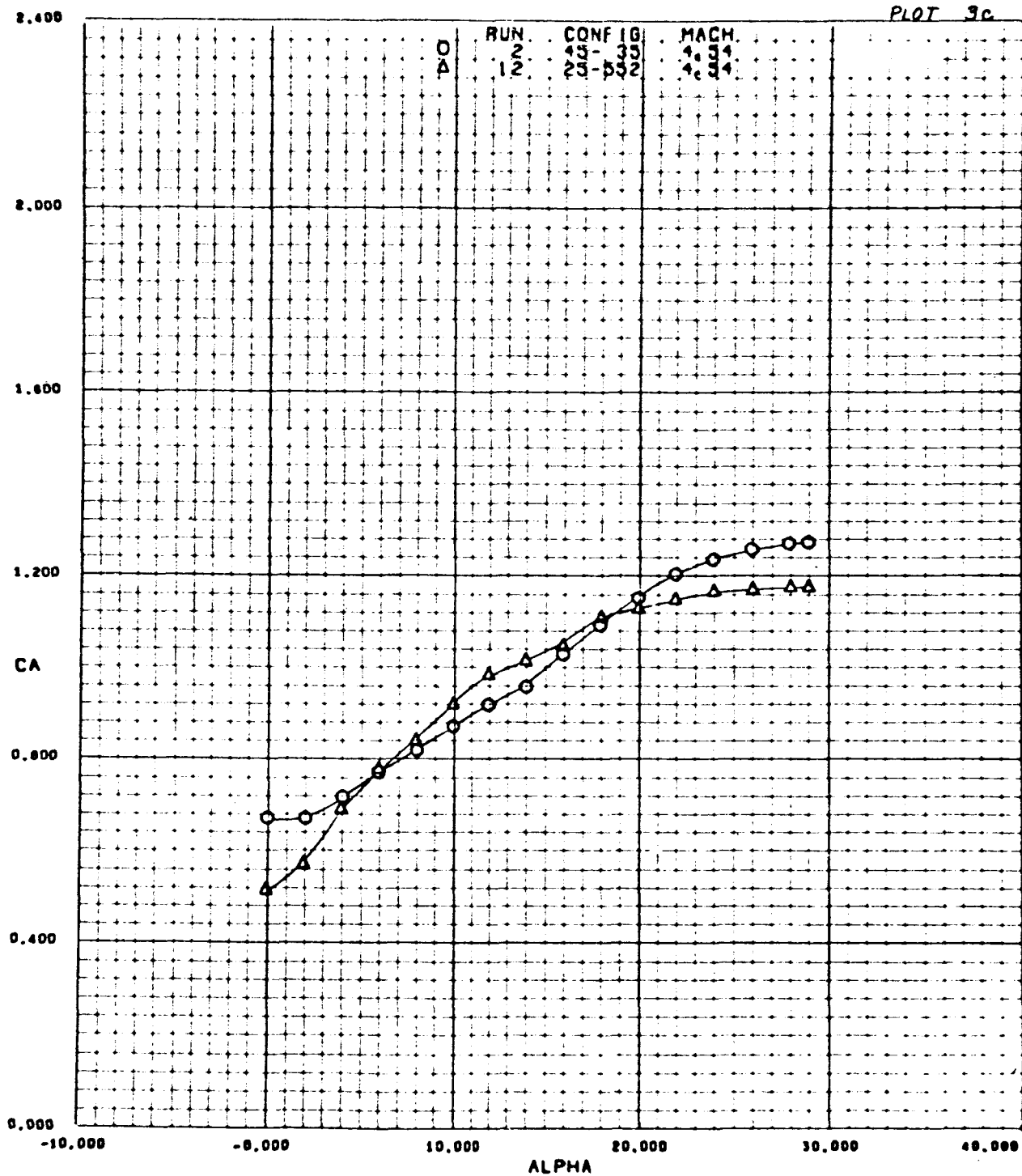




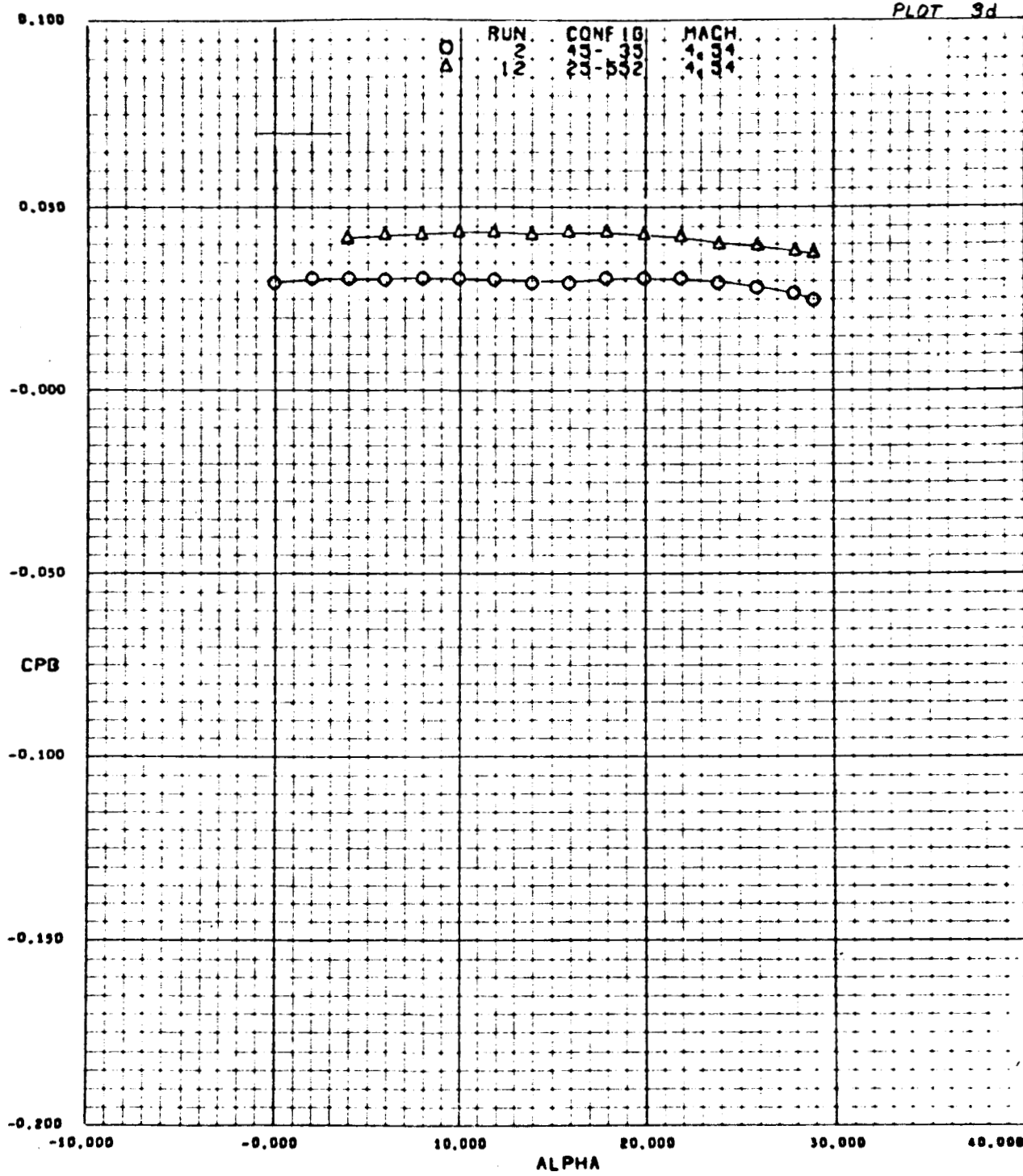
PLOT 3b



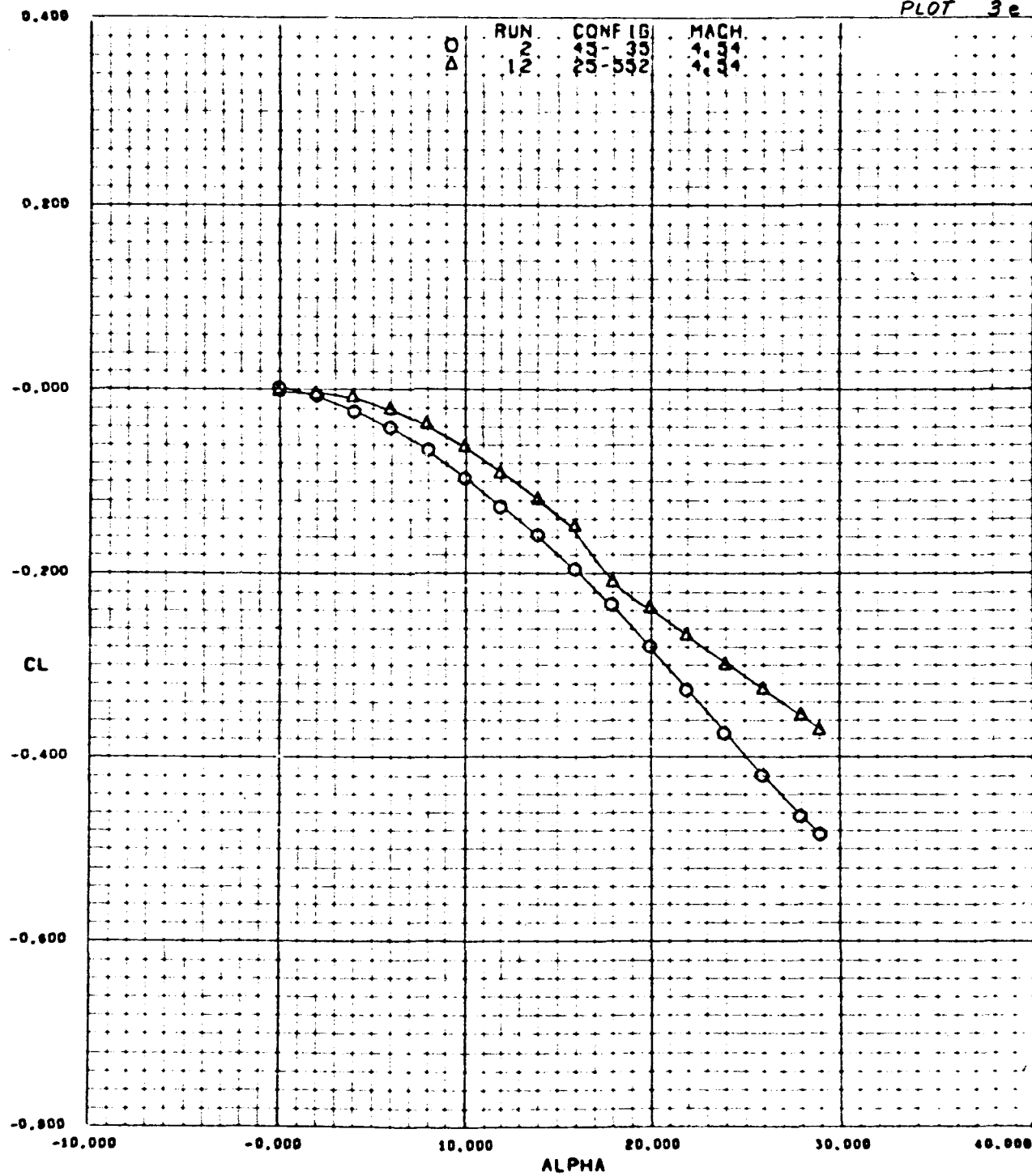
PLOT 3C



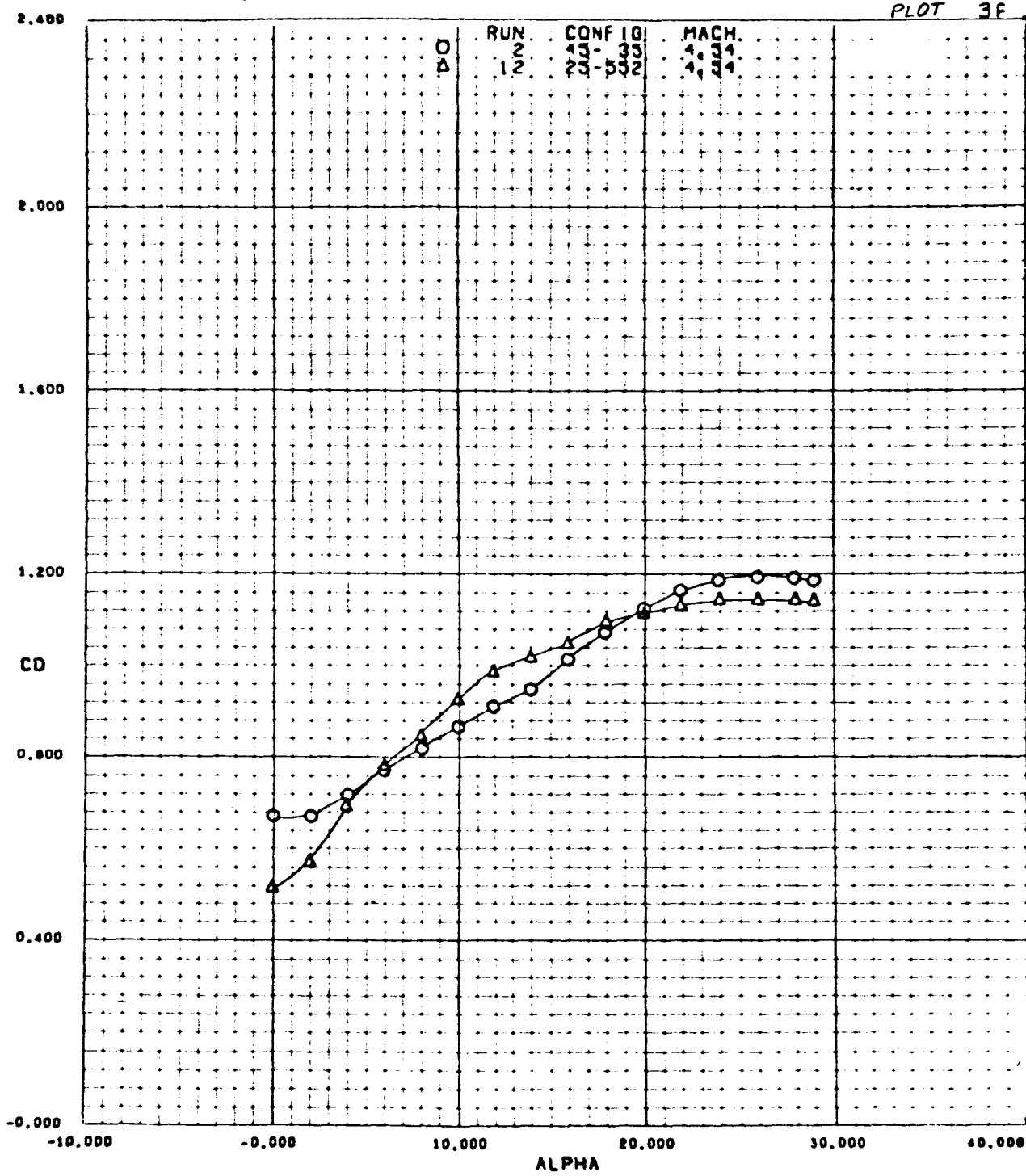
PLOT 3d



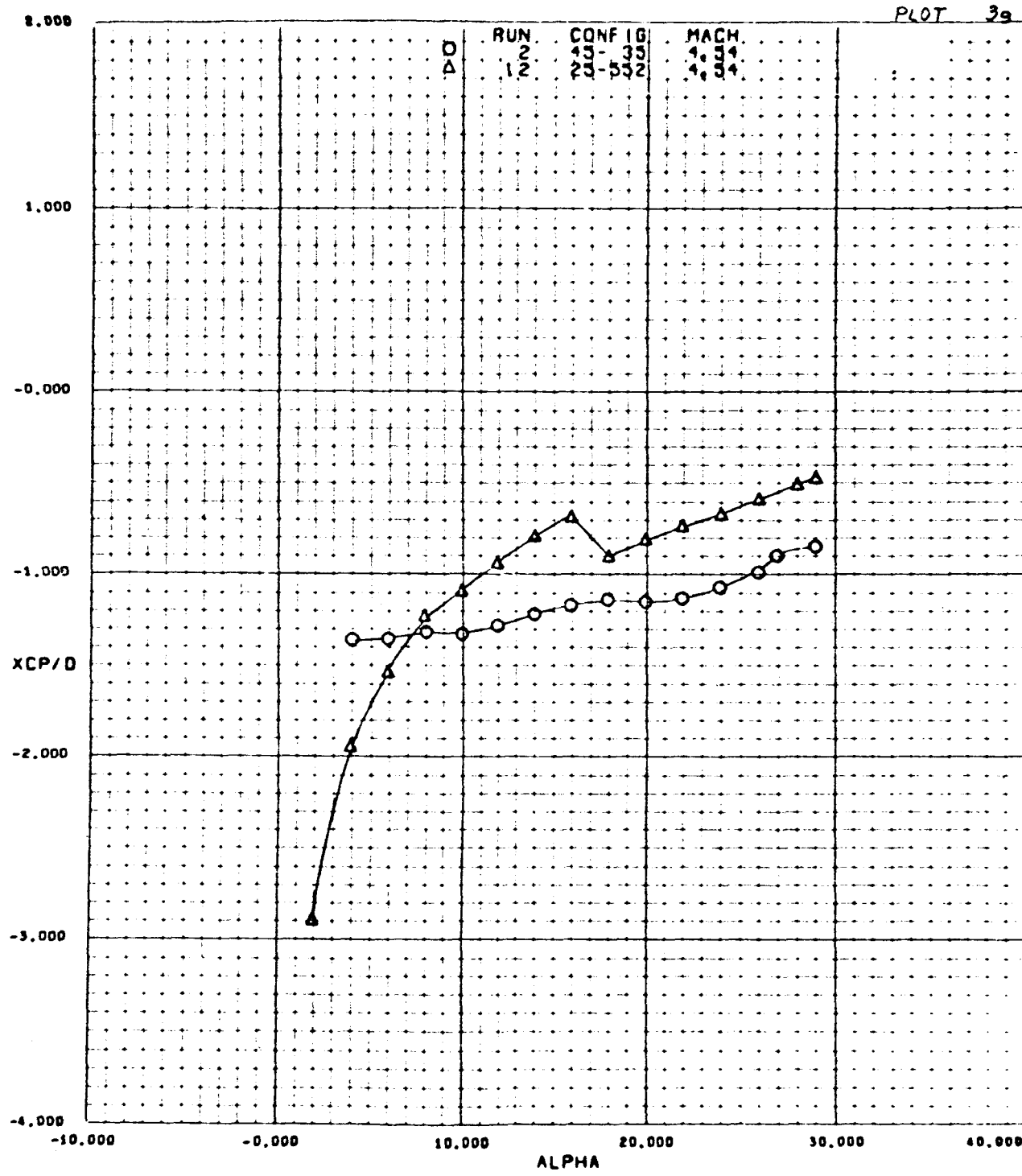
PLOT 3e



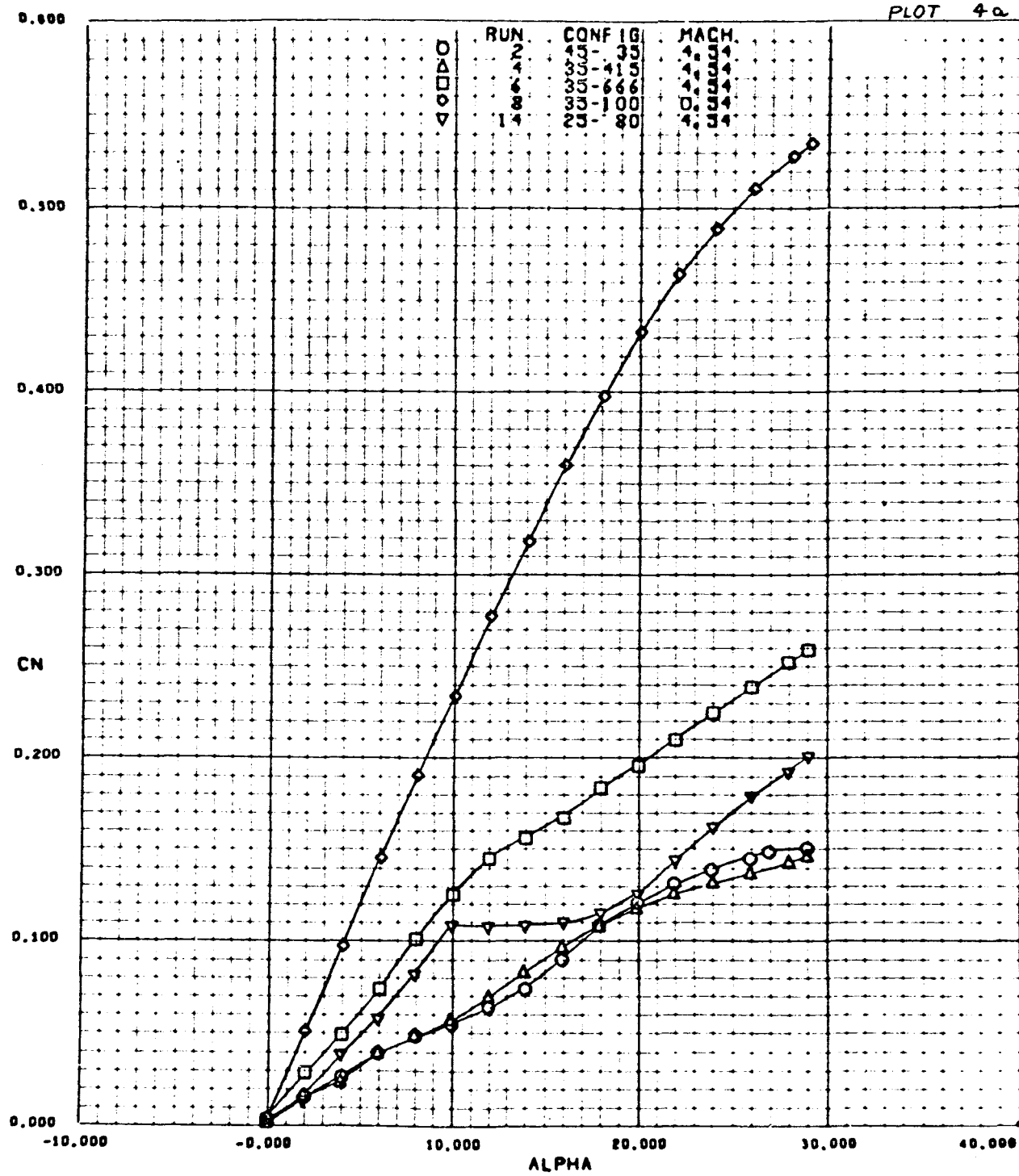
PLOT 3F



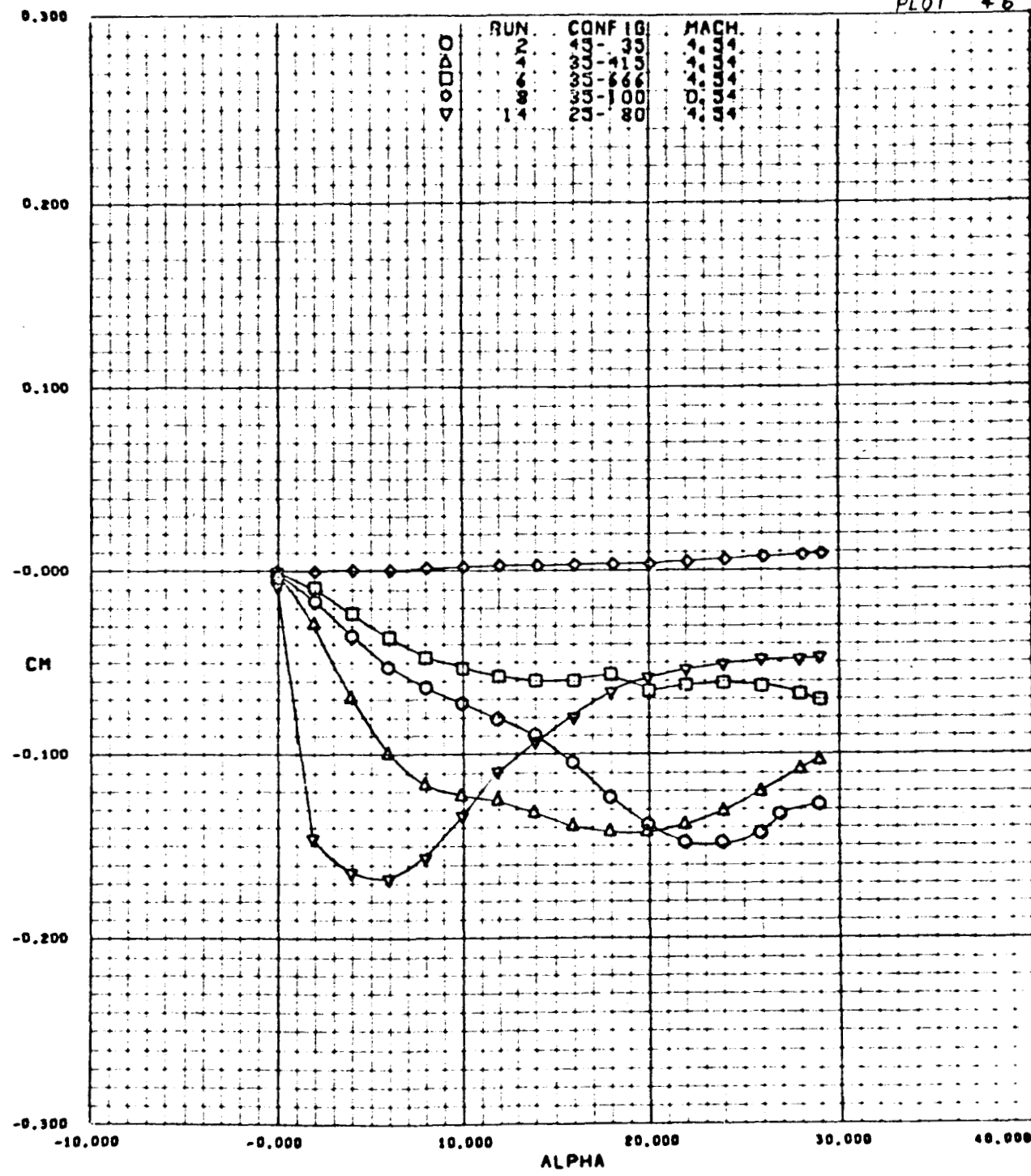
JPL WT 20-565



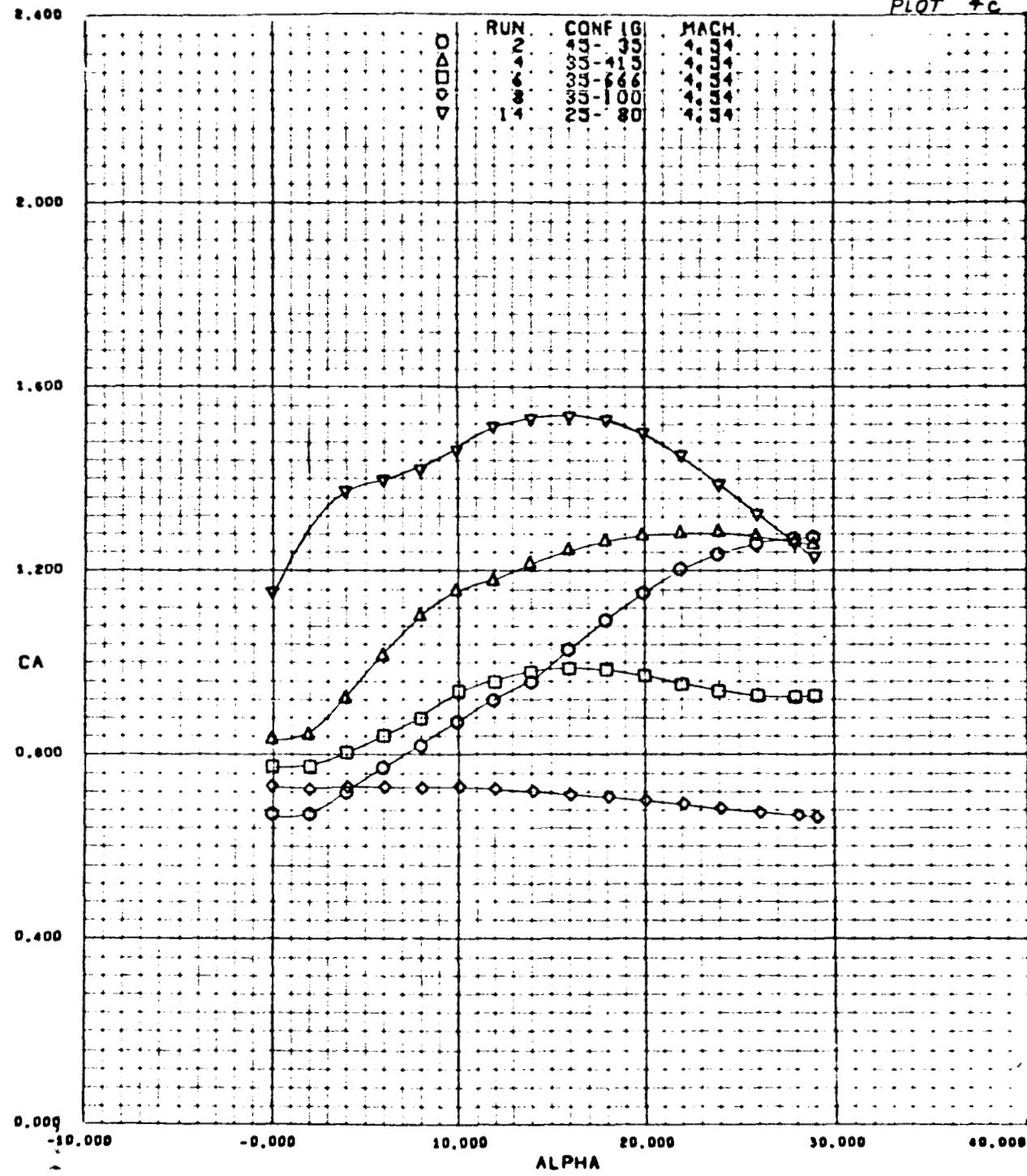
PLOT 4a



PLOT 4b

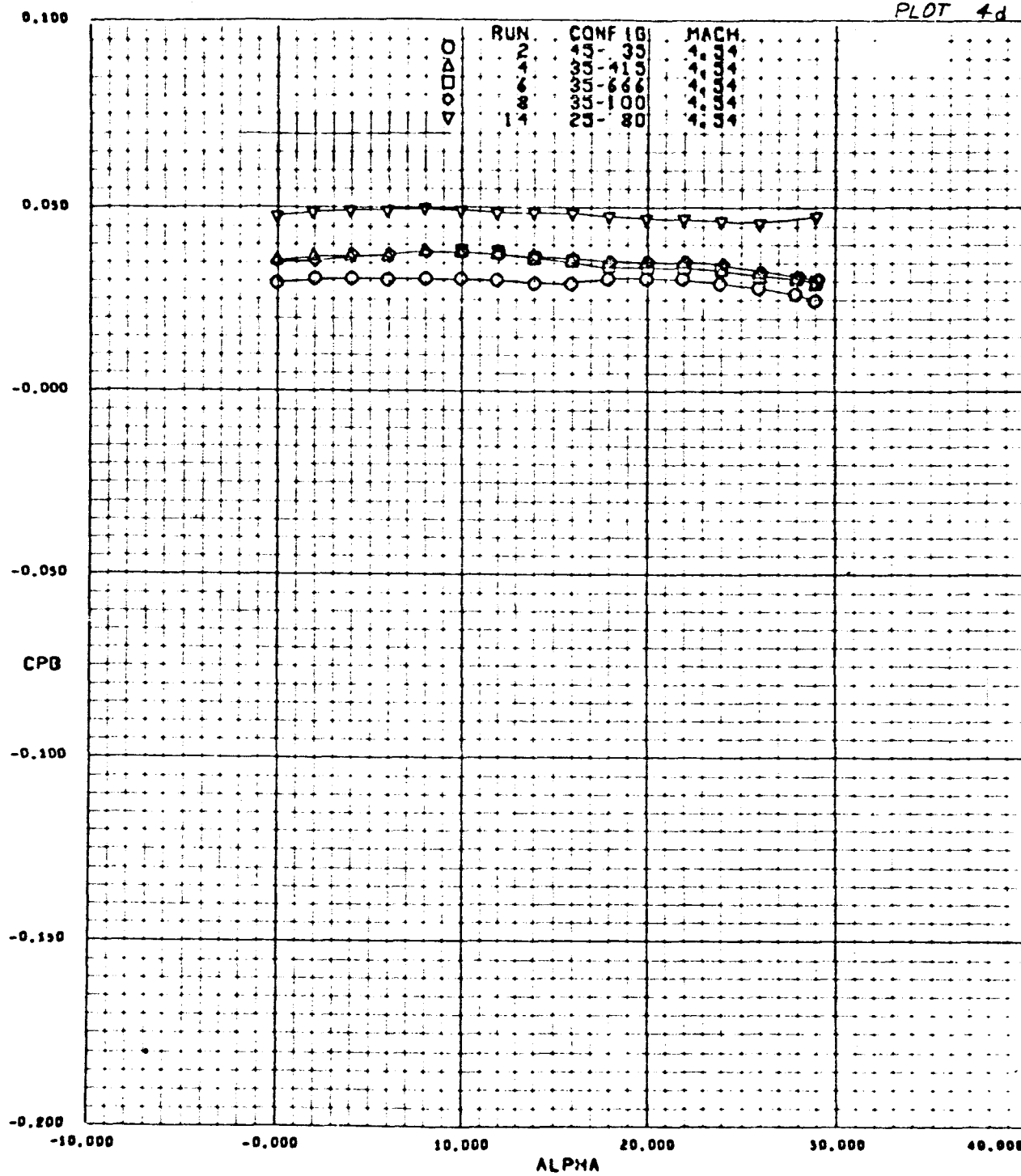


PLOT 4C

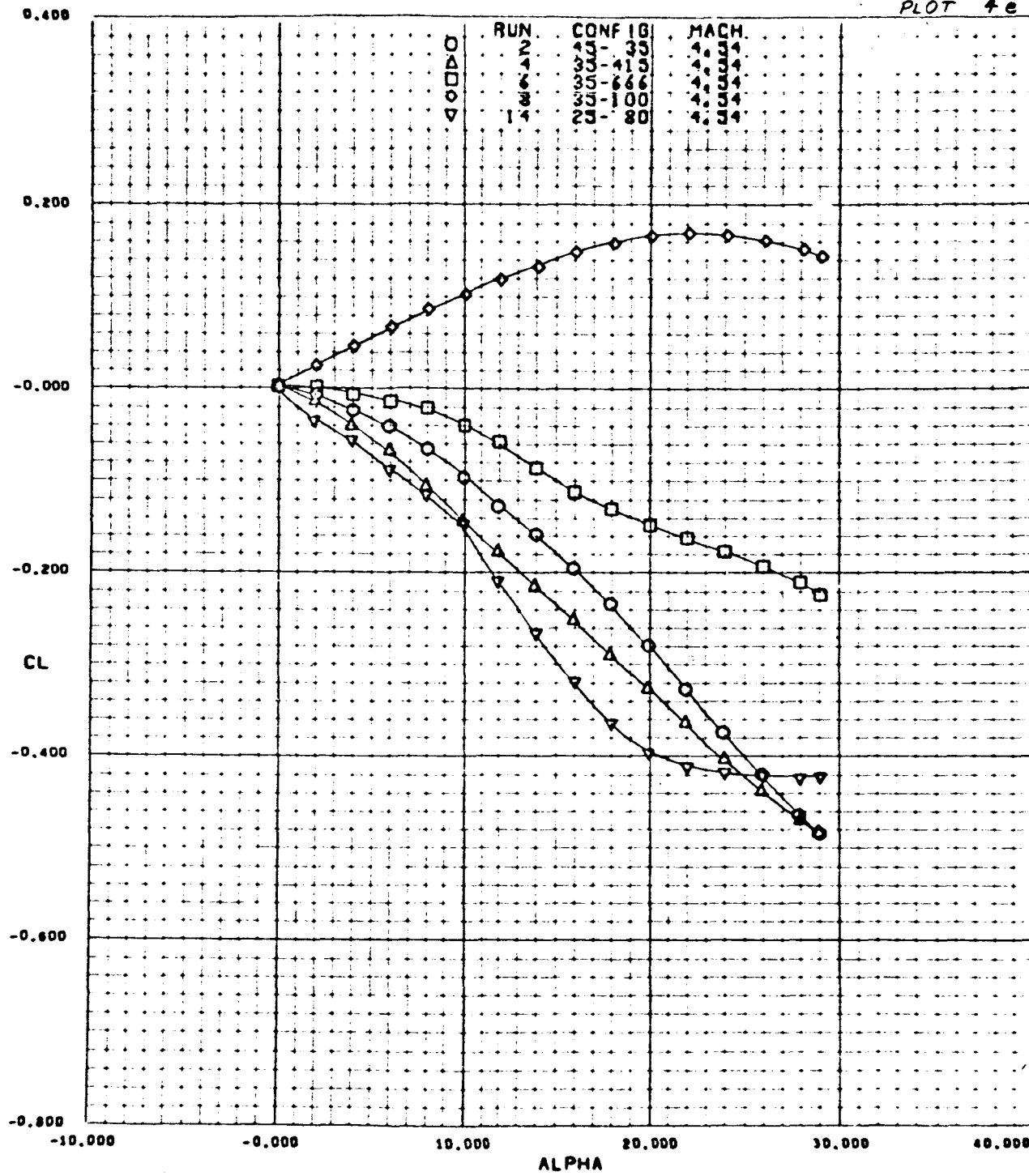


JPL WT 20-565

PLOT 4d



PLOT 4e



PLOT 4F

